



**VICTORIA UNIVERSITY**  
MELBOURNE AUSTRALIA

*Evaluation of long-term operational and treatment performance of a high-biomass submerged anaerobic membrane bioreactor treating abattoir wastewater*

This is the Published version of the following publication

Gautam, Rajneesh Kumar, Olubukola, Akangbe, More, Nandkishor, Jegatheesan, Veeriah, Muthukumaran, Shobha and Navaratna, Dimuth (2023) Evaluation of long-term operational and treatment performance of a high-biomass submerged anaerobic membrane bioreactor treating abattoir wastewater. *Chemical Engineering Journal*, 463. ISSN 1385-8947

The publisher's official version can be found at  
<https://www.sciencedirect.com/science/article/pii/S1385894723008768>  
Note that access to this version may require subscription.

Downloaded from VU Research Repository <https://vuir.vu.edu.au/45662/>



# Evaluation of long-term operational and treatment performance of a high-biomass submerged anaerobic membrane bioreactor treating abattoir wastewater

Rajneesh Kumar Gautam<sup>a</sup>, Akangbe Olubukola<sup>b</sup>, Nandkishor More<sup>c</sup>, Veeriah Jegatheesan<sup>d</sup>, Shobha Muthukumar<sup>a</sup>, Dimuth Navaratna<sup>a,e,\*</sup>

<sup>a</sup> Institute for Sustainable Industries & Liveable Cities, College of Engineering and Science, Victoria University, Melbourne, VIC 3011, Australia

<sup>b</sup> École Spéciale de Mécanique et d'Électricité (ESME Sudria), Paris, France

<sup>c</sup> School of Earth and Environmental Science, Department of Environmental Science, Babasaheb Bhimrao Ambedkar University, Lucknow 226025, India

<sup>d</sup> School of Engineering and Water: Effective Technologies and Tools (WETT) Research Centre, RMIT University, Melbourne, VIC 3000, Australia

<sup>e</sup> ITCGU, Faculty of Engineering, University of Peradeniya, Prof. E. O. E. Pereira Mawatha, Kandy 20000, Sri Lanka

## ARTICLE INFO

### Keywords:

High biomass AnMBR  
Abattoir wastewater  
membrane fouling, extracellular polymeric substance (EPS), soluble microbial products (SMP)  
sustainable organic loading rate (OLR)

## ABSTRACT

Although anaerobic membrane bioreactors (AnMBR) are widely used in high-strength wastewater treatment and resource recovery, membrane operational performance and membrane fouling control remain critical issues. In this study, the operational and treatment performance of a high-biomass ( $18 \leq \text{MLSS (g/L)} \leq 35$ ) submerged anaerobic membrane bioreactor (HBSAnMBR) was assessed at organic loading rates (OLR) of 1.05–5 kg-COD/m<sup>3</sup>/d to treat abattoir wastewater (AWW). The correlation between kinetic parameters representing biomass yield and extracellular polymeric substances (EPS) was thoroughly investigated using mathematical models. It was found that the yield of biomass and EPS correlated positively with applied OLR and were found in the range of 0.13–0.31 g-MLSS/g-COD and 0.00001–0.000013 g-EPS/g-MLSS, respectively. This study also systematically examined the cake layer fouling mechanisms of HBSAnMBR due to EPS and the influence of soluble microbial products (SMP) on membrane pore blocking. OLR above 4 kg-COD/m<sup>3</sup>/d negatively affected the performance in terms of TMP, filtration resistance, EPS/SMP production, and COD removal suggesting that HBSAnMBR can be operated sustainably at OLR 4 kg-COD/m<sup>3</sup>/d. The membrane autopsy analyses and foulant characterization found that cake layer foulants were primarily composed of polysaccharides and proteins, while the membrane did not experience pore-blocking. At the same time, sodium, phosphorous, and calcium triggered inorganic fouling. The efficient treatment of abattoir wastewater showed that the HBSAnMBR system could be applied to treat trade wastewater containing high-organic content.

## 1. Introduction

The abattoir industry consumes a significant amount of water, which becomes contaminated with organic pollutants and nutrients while undergoing different slaughtering activities. As a result, they become an excellent candidate for advanced treatment processes to recover energy and nutrient resources. The generated wastewater is often called trade wastewater [1], which consists of high: turbidity, total suspended solids

(TSS), chemical oxygen demand (COD), total nitrogen (TN), total phosphorus (TP) concentrations, and elevated levels of organic matter (Protein and blood), including fats, oils, and greases (FOG) [2]. Generally, the FOG from abattoir wastewater is removed using sorption [3], mechanical skimmers [4] and traditional approaches, which include injecting bacteria or enzymes [5] prior to advanced treatment. However, entering a municipal wastewater treatment system into the other untreated organic components of abattoir wastewater, such as TSS, COD, TN, and TP, may create severe environmental constraints and incur huge

**Abbreviations:** AD, Anaerobic Digestion; ANOVA, Analysis of Variance; AWW, Abattoir Wastewater; CI, Confidence Interval; COD, Chemical Oxygen Demand; EPS, Extracellular Polymeric Substances; HBSAnMBR, High Biomass Submerged Anaerobic Membrane Bioreactor; HRT, Hydraulic Retention Time; MLSS, Mixed Liquor Suspended Solids; MLVSS, Mixed Liquor Volatile Suspended Solids; ODE, Ordinary Differential Equation; OLR, Organic Loading Rate; SMP, Soluble Microbial Products; SRT, Solid Retention Time; TMP, Transmembrane Pressure; UF, Ultrafiltration.

\* Corresponding author.

E-mail address: [dnavaratna@pdn.ac.lk](mailto:dnavaratna@pdn.ac.lk) (D. Navaratna).

<https://doi.org/10.1016/j.cej.2023.142145>

Received 8 December 2022; Received in revised form 17 February 2023; Accepted 23 February 2023

Available online 28 February 2023

1385-8947/© 2023 The Authors. Published by Elsevier B.V. This is an open access article under the CC BY-NC-ND license (<http://creativecommons.org/licenses/by-nc-nd/4.0/>).

**Nomenclature**

Symbol Description Unit

$\mu$	Viscosity of permeate	Pa.s
EPSc	Carbohydrate concentration in EPS	g/L
EPSp	Protein concentration in EPS	g/L
$j$	Flux	L/m <sup>2</sup> /hr
$k_{dm}$	Detachment rate of EPS	/d
$k_{dp}$	Decay rate of EPS	/d
$k_{dx}$	Biomass decay rate	/d
$L$	Organic loading rate (OLR)	kg-COD/m <sup>3</sup> /d
$m$	EPS density on the membrane surface	kg/m <sup>2</sup>
$p$	Concentration of total EPS in AnMBR mixed liquor	g/L
$R_c$	Resistance due to cake-layer	1/m
$R_{cp}$	Concentration polarization resistance	1/m
$R_m$	Intrinsic membrane resistance	1/m

$R_t$	Total filtration resistance	1/m
SMPc	Carbohydrate concentration in SMP	g/L
SMPp	Protein concentration in SMP	g/L
$T$	Time	d
$V$	Hydraulic volume of the bioreactor	L
$x$	MLSS concentration in the bioreactor	g/L
$Y$	Yield coefficient of biomass	g-MLSS/g-COD
$\beta$	Yield coefficient of EPS	g-EPS/g-MLSS
$\delta$	EPS biofilm thickness	m
$\gamma$	Coefficient of EPS fouling	/d
$\Delta_m$	Static friction coefficient	-
$\Delta P$	Transmembrane pressure	Pa
$\varepsilon$	Deposit porosity	-
$\sigma$	SMP fraction retained by the membrane	-
$\tau_m$	Shear stress	Pa

levies for the trade waste generators, including penalties.

The most common physicochemical pretreatment methods for abattoir wastewater (AWW) treatment have dissolved air floatation (DAF) and coagulation-flocculation [6]. However, these methods consume energy, demand excessive chemicals, and still perform poorly, with 30 % and 60 % COD reductions, respectively, yet inefficiently reducing organic loading. Recently, activated sludge treatment [7], constructed wetlands [8], and sequential batch reactors (SBR) [9] have been researched extensively for AWW treatment. However, their application to AWW was deemed unsustainable due to their large space requirements and higher footprints.

It is remarkable that conventional anaerobic system in AWW treatment, such as anaerobic lagoons [10] and an up-flow anaerobic sludge blanket (UASB), has been studied extensively for treating AWW and proven effective. Nevertheless, lagoon-based technologies have significant drawbacks [11], including their comparatively large footprints, low resource recovery affinities, unpleasant odours, and costly desludging techniques. Similarly, UASB and other granule-based systems are extremely sensitive to lipids [12], while they are moderately sensitive to other organic solids demanding effective pretreatment. In the last decade, several anaerobic processes tolerant of fat and high organic solids have been researched extensively, including anaerobic flotation reactor (AFR) [13], anaerobic sequencing batch reactor (ASBR) [14], anaerobic baffled reactor (ABR) [15], and anaerobic membrane bioreactor (AnMBR) [16,17]. Among these, AnMBR has gained attention and has been extensively researched as the most appropriate high-rate anaerobic pretreatment (HRAPT) for the pretreatment of food industrial wastewaters at organic loading ranging from 1.5 kg-COD/m<sup>3</sup>/d [18] to 22.57 kg-COD/m<sup>3</sup>/d [19], including confectionery [20], semi-solid food waste [19], breweries [21], dairy [22], seafood [23], beet molasses [24], cheese and whey [25], wineries [26], and swine wastewaters [27]. Subsequent interest has centred on investigating the performance of a high-biomass submerged anaerobic membrane bioreactor (HBSAnMBR), operating at a biomass concentration of over 15 g/L to treat a wide variety of wastewater originating from industrial and municipal solid wastes to several agricultural-food waste products [28].

AnMBR incorporates the anaerobic-biological-membrane separation processes in a single unit and possesses potential advantages, including; operating at high organic loading rates, low space-energy requirements [29], ability to disengage solid retention time (SRT) and hydraulic retention time (HRT) [30], complete retention of biomass, superior treatment performance and tri-resource recovery [31]. However, the most significant barrier to the widespread use of the AnMBR system is the “fouling of the membrane”, which limits its widespread full-scale application. The key parameters that govern the fouling of the membrane are not limited to; the characteristic of the membrane [32], the

configuration of AnMBR [33], substrate composition [34], biomass concentration [35], the concentration of extracellular polymeric substances (EPS) and soluble microbial products (SMP) [36] and the organic loading rate (OLR) [37]. Of these, OLR has a significant role in the contribution to the fouling of the membrane, which in turn could increase microbial growth, leading to an increase in EPS and SMP concentrations [38]. However, several studies mention that increased OLR promotes bacterial growth, resulting in more stabilized treatment and improved filtration performance with active biomass retention by the membrane [39]. Due to diverse opinions on OLR, the concept of sustainable OLR has been researched to investigate the optimum OLR at which the AnMBR operates sustainably for effluents, such as confectionery [20], municipal wastewater [40], food waste [41] and synthetic antibiotics [39]. Most of these studies were conducted at  $6 \leq \text{MLSS (g/L)} \leq 18$ . However, no study has reported systematically conducted research on investigating the sustainable range of OLR for a long-term operation of a submerged AnMBR treating abattoir wastewater (AWW) under extremely high biomass concentrations ( $18 \leq \text{MLSS (g/L)} \leq 35$ ).

In summary, this study critically investigated the performance of a high-biomass submerged AnMBR (HBSAnMBR) coupled with UF ceramic membrane treating AWW at various OLRs. The experimentally obtained results were evaluated using numerical models previously developed by Gautam et al. [31,42]. The critical operational parameters governing the fouling mechanism in the HBSAnMBR and the time-based MLSS, EPS, and SMP concentrations and subsequent filtration resistance and TMP variations at various OLR ranges were thoroughly evaluated. The treatment performance using COD, TN, and TP were assessed during the long-term HBSAnMBR operation. Additionally, membrane morphology and cake-layer foulants were analyzed using SEM-EDX and FTIR spectroscopy. The findings of this study provide a control strategy to reduce membrane fouling by providing a scientific rationale for the sustainable operation of an HBSAnMBR treating trade wastewater generated from abattoirs.

## 2. Material and methods

### 2.1. High-biomass submerged anaerobic membrane bioreactor (HBSAnMBR) experimental setup

A detailed schematic diagram of the lab-scale HBSAnMBR experimental setup is illustrated in Fig. 1. It consists of a water-jacketed, continuously stirred glass fermenter (bioreactor) vessel of 5 L hydraulic capacity with a working volume of 3.5 L with a headspace of 1.5 L. The HBSAnMBR was operated using a BIostat® automated controller (Applikon Bio Console ADI 1035) that controls the feed flow, stirrer

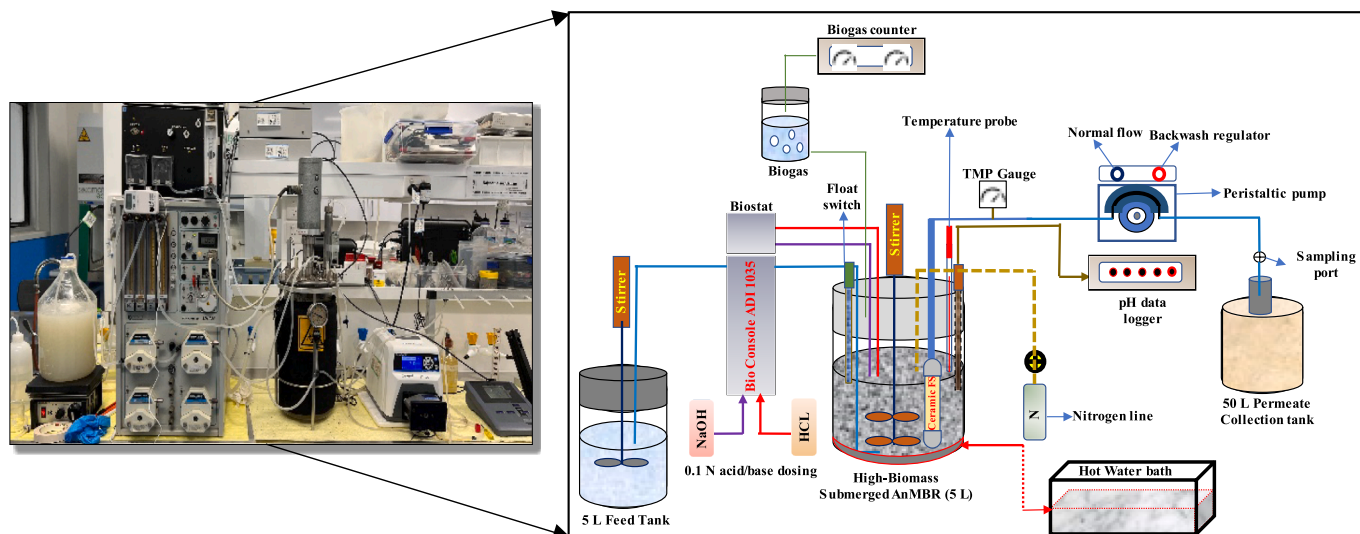


Fig. 1. A schematic diagram of a high-biomass submerged AnMBR (HBSAnMBR) setup.

speed, and pH. An electromechanical float switch (Jaycar-SF0920) attached to HBSAnMBR was connected to the BIOSTAT® to draw the abattoir wastewater from a 5 L PVC feed storage tank using a peristaltic pump (Masterflex 7518-00) attached to the BIOSTAT®. In contrast, a 50 L PVC container collected the HBSAnMBR-treated permeate through a high-precision peristaltic precision pump (Masterflex L/s 07551-20). Strict anaerobic and mesophilic conditions ( $35 \pm 2.5$  °C) were maintained in the HBSAnMBR using a nitrogen gas line and a hot water bath attached to the bioreactor. To maintain a neutral pH level in the HBSAnMBR system, a pH regulator system (Platon) connected to the BIOSTAT® via a pH probe (Mettler Toledo) was used, which injected the acid/alkali solutions (0.1 M HCl) and base (0.1 M NaOH) using dosing pumps (Masterflex 7518-00). The inoculum was suspended by maintaining consistent and thorough stirring using a mechanical stirrer attached to the HBSAnMBR and controlled using the BIOSTAT®. A negative pressure gauge (Ambitinst Australia) was used to monitor the transmembrane pressure (TMP) while connected to the membrane outlet and peristaltic precision pump (Masterflex L/s 07551-20).

A ceramic flat-sheet ultrafiltration (UF) membrane module supplied by GuoChu Tech Xiamen, China, was submerged in the bioreactor to separate the biomass and produce high-quality treated effluent using a peristaltic precision pump (Masterflex L/s 07551-20). The ceramic UF membrane module had an outer surface dimension of  $0.117 \times 0.015 \times 0.126$  m and an active surface dimension of  $0.086 \times 0.006 \times 0.110$  m with an effective filtration area of  $0.02$  m<sup>2</sup>. The critical membrane specifications were; Composition: Al<sub>2</sub>O<sub>3</sub> (base material), titanium (housing material), and silicon (sealing material); filtration mode: out-in; nominal pore size: 0.1 μm; maximum operational temperature: 60 °C; particle removal  $\geq 100$  nm, operational pH range: 2–12; and hydrophobic. The membrane was physically cleaned following the protocol mentioned by Navaratna et al. [43] and by adopting the manufacturer's (GuoChu Tech, Xiamen) chemical cleaning protocol by immersing, bubbling, and backwashing the membrane using 3 g/L of NaClO, followed by backwashing the membrane with MiliQ ultrapure water to remove the NaClO residues.

## 2.2. Experimental conditions

### 2.2.1. Abattoir wastewater characteristics

The simulated abattoir wastewater was prepared based on the reported real wastewater composition [11] for HBSAnMBR operation according to the recipe described in Table 1. These feed samples for a quantity of 5 L were prepared in powdered form, stored in 250 g

Table 1

Simulated abattoir wastewater recipe.

Macro Nutrients	Concentration (g/L)	5 L (g)
Anhydrous Sodium Acetate (NaCH <sub>3</sub> COOH·3H <sub>2</sub> O)	1.75	8.75
Soy Protein	1.75	8.75
Glucose (C <sub>6</sub> H <sub>12</sub> O <sub>6</sub> )	5.0	25
Urea (CH <sub>4</sub> N <sub>2</sub> O)	0.35	1.75
Potassium Dihydrogen Phosphate (KH <sub>2</sub> PO <sub>4</sub> )	0.5	2.5
Magnesium Sulphate (MgSO <sub>4</sub> ·7H <sub>2</sub> O)	0.35	1.75
Calcium Chloride (CaCl <sub>2</sub> ·2H <sub>2</sub> O)	0.5	2.5
Micro Nutrients (ml)	0.35	1.75

polyethylene zipper bags, and preserved at 4 °C to reduce decay. The simulated wastewater had a COD of  $8300 \pm 300$  mg/L, TN of  $450 \pm 20$  mg/L, TP of  $490 \pm 30$  mg/L and an acidic character with a pH of  $4.81 \pm 1.5$ . Before the wastewater was fed into the reactor, the pH of the stock feed was adjusted to  $7 \pm 0.5$  using 0.1 N NaOH. The feed was purged with 0.5 L/min nitrogen gas for 3 min to remove the dissolved oxygen to ensure strict anaerobic conditions in the HBSAnMBR. For a diluted sample equivalent to 5 L, the chemical compounds used to supply micronutrients and cations required for the anaerobic treatment [44] were added as per the recipe shown in Table S1.

### 2.2.2. Inoculum characteristics

The inoculum was collected from a mesophilic anaerobic digester of a paper and pulp wastewater treatment facility known as Gippsland Water Factory (GWF) in Victoria, Australia. The bioreactor was acclimated using simulated abattoir wastewater, as shown in Table 1. The mixed liquor suspended solids concentration (MLSS), and the mixed liquor volatile suspended solids (MLVSS) of undiluted inoculum were 65.85 g/L and 57.29 g/L, respectively. The HBSAnMBR was commissioned at a dilution ratio of 3:7 (substrate: inoculum). The bioreactor was occasionally purged with nitrogen gas (0.5 L/min) for 5 min to ensure strict anaerobic conditions in the HBSAnMBR.

## 2.3. HBSAnMBR operation

The HBSAnMBR was continuously operated under different operating conditions in 7 distinct phases consisting of acclimatization (Phases 1a, 1b, 2a, and 2b), transition (Phase 3), and stabilization Phases (4 and 5) for 125 days, as shown in Table 2. The biomass concentration was intentionally kept high ( $18 \leq \text{MLSS (g/L)} \leq 35$ ) during the acclimatization period to investigate biomass concentration change due to

**Table 2**  
HBSAnMBR operating conditions.

Phase	Days of operation	MLSS (g/L)*	MLVSS (g/L)*	OLR (kg-COD/m <sup>3</sup> /d)	Flux (LMH)	HRT (days)
1a	0–14	34.31	29.12	1.05	3.0	3.35
1b	15–29	23.10	18.65	1.45	3.6	2.90
2a	30–44	19.46	15.82	1.72	4.5	2.30
2b	45–64	18.72	15.87	2.40	7.5	1.39
3	65–84	24.30	18.49	3.20	10.0	1.00
4	85–109	20.82	15.96	4.00	12.5	0.83
5	110–125	19.37	14.30	5.00	15.0	0.69

\*average value through the phase.

OLR. To mitigate heavy fouling and observe the system's performance, the initial OLR during Phases 1a, 1b, 2a and 2b were kept as low as 1.05, 1.45, 1.72, and 2.40 kg-COD/m<sup>3</sup>/d, respectively. However, during the consecutive Phases: 3, 4 and 5, the OLR was methodically increased to 3.2, 4, and 5 kg-COD/m<sup>3</sup>/d, respectively, to observe the system's performance. During Phases 1a, 1b, 2a, 2b, and 3–5, suction rates were regulated by adjusting the flow rate to obtain the designed OLR values. The HBSAnMBR was operated in 30-min cycles (2 cycles per hour), consisting of 25 min of filtration and 5 min of high-intensity backwash (three times of suction rate). The average operational flux during Phases 1a, 1b, 2a, 2b, 3, 4, and 5 was 3, 3.6, 4.5, 7.5, 10, 12.5, and 15 L/m<sup>2</sup>/hr (LMH), respectively, resulting in a decreased HRT from 3.35 d (Phase 1a) to 0.69 d (Phase 5). The reactor was operated at a controlled temperature of 35 °C, pH of 7 ± 0.25 and a 140 rpm stirring speed.

#### 2.4. Detailed analytical procedure

The physicochemical parameters such as COD, TN, and TP were analyzed in DR 5000™ UV-Vis Spectrophotometer using standard colorimetric methods [45]. The MLSS and MLVSS concentrations of bioreactor sludge samples were measured using standard methods [45]. Navaratna et al. [37] described a method for EPS extraction in the aerobic MBR study, which was slightly modified in this study. Initially, a 20 mL sample of mixed liquor was allowed to settle for 1 h at 4 °C, and the supernatant was removed. The settled sediment/sludge was then diluted with 8 mL of MilliQ ultrapure water and carefully kept in a mechanical shaker for 5 min at 150 rpm. The diluted sludge mixture was centrifuged at 13200 rpm (12225g) for 20 min at 4 °C to collect the supernatant, known as soluble microbial products (SMP). The remaining sludge was then re-suspended in 8 mL of 0.1 N NaOH solution and mixed thoroughly in the same mechanical shaker at 150 rpm for 120 min before being centrifuged at 13,000 rpm (11337g) for 20 min at 4 °C to give the EPS concentration. The SMP and EPS samples were then neutralized with 0.1 N HCl.

The phenol-sulphuric acid method [46] was used to determine carbohydrate (polysaccharide) concentrations, with glucose as a control. The protein concentration in the EPS and SMP was measured using the ThermoScientific Modified Lowry Protein Assay Kit (23240), which contains Folin-Ciocalteu Reagent and the Lowry original reagent. Bovine Serum Albumin (BSA) (1–1500 mg/L) from the modified Lowry Protein Assay Kit was utilized as a standard to create the calibration curve. The samples were examined for absorbance using a UV-2600 UV/vis double-beam spectrometer set to a wavelength of 490 nm for polysaccharides or 750 nm for proteins, and the concentrations of all samples were determined.

##### 2.4.1. Membrane morphology and foulant characterization

**Fourier transmission infrared spectroscopy (FTIR) analysis:** FTIR with gas cell (Perkin Elmer) was used to investigate the surface properties and detect the functional groups on the cake layer and the membranes (clean and fouled) between the wavenumber of 500 and 4000/cm. The cleaned and fouled membranes and the cake-layer

foulants scrapped from the membrane surface were thoroughly dried in a hot air oven at 70 °C for 48 h to remove moisture and kept for 24 h in a desiccator before analysis. The FTIR analysis of the fouled membranes and the cake layer was performed during Phases 1a, 1b, and 3.

**Field emission scanning electron microscope (FESEM):** A (FESEM) (ThermoFisher Scientific) was used to examine the surface morphology of the ceramic UF flat-sheet membrane and the membrane foulants (cake layer). Before testing, the membrane samples were cut using a ceramic cutter and then coated with sputtering platinum. FESEM photomicrographs of the cross-section and the outer surface of selected samples were taken at a magnification of 5000x and 9000x.

**Energy-dispersive X-ray (EDX) analysis:** EDX analyzer (ThermoFisher Scientific) was used to characterize the elemental-chemical compositions in the cake layer.

#### 2.5. Parameter estimation using numerical models

The mathematical model equations developed by Gautam et al. [31], Charfi et al. [47] and Olubukola et al. [42] were used to estimate the kinetic parameters and simulate the time-based variation of MLSS, EPS, TMP, and  $R_t$  (total resistance). The nomenclature defines the lists of the parameters with their symbols. The Runge-Kutta 4th order differential equation (ODE) was used at a step size of 0.05 to simulate the model equations (Equations (1), 2, 3, and 6). The model input parameters were taken from the literature and are summarised in Table 3.

##### 2.5.1. Biomass concentration in the HBSAnMBR

The change in concentration of the biomass during Phases (1a, 1b, 2a, 2b, 3–5) was simulated to obtain the coefficient of biomass yield ( $Y$ ) and decay rate ( $K_{dx}$ ) using Equation (1) [31,51].

$$\frac{dx}{dt} = YL - k_{dx}x \quad (1)$$

Where  $x$  is the concentration of biomass (MLSS),  $Y$  is biomass yield due to substrate consumption in (g-MLSS/g-COD), and  $K_{dx}$  is the decay rate of biomass in (/d). The growth of biomass due to influent COD is expressed as  $YL$ . Where  $L$  is the organic loading rate (OLR) (kg-COD/m<sup>3</sup>/d).

##### 2.5.2. EPS concentration in the HBSAnMBR

The change in concentration of EPS during Phases (1a, 1b, 2a, 2b, 3–5) was simulated to obtain the coefficient of EPS yield ( $\beta$ ) and decay rate ( $k_{dp}$ ) using Equation (2) [31,42].

$$\frac{dp}{dt} = \beta(YL) - k_{dp}(p) \quad (2)$$

where  $p$  is the EPS concentration in the HBSAnMBR mixed liquor (g/L),  $\beta$  is EPS yield in (g-EPS/g-MLSS), and  $K_{dp}$  is the decay rate of EPS in (/d).

**Table 3**  
Model input parameters.

Symbol	Description	Unit	Initial values	Reference
$Y$	Yield coefficient of biomass	g-MLSS/g-COD	0.08	[48]
$K_{dx}$	Biomass decay rate	/d	0.037	[49]
$K_{dp}$	Decay rate of EPS	/d	0.020	[50]
$\eta$	Constant	1/d-Pa	0.1	[51]
$\tau_m$	Shear stress	Pa	5.0	[37]
$\beta$	Yield coefficient of EPS	g-EPS/g-MLSS	0.01	[31]
$\Delta m$	Static friction constant	unitless	$1 \times 10^{-3}$	[31]
$k_e$	Coefficient of deposit porosity decrease	–	$1 \times 10^{-3}$	[47]
$\alpha$	Specific resistance of the cake	1/m	$1.20 \times 10^{12}$	[42]

$\mu$  was taken as 0.001 (Pa.s) as that of pure water.

Using model equations by Gautam et al. [31] in their AnMBR study, the EPS density was modelled, considering the accumulation of EPS ( $m$ ) (Equation (3) due to advection force (out-in filtration) and detachment (Equation (4) as a result of shear-induced from backwashing (Equation (5)).

$$\frac{dm}{dt} = Jp - k_{dm}m \quad (3)$$

where  $J$  is the flux through the membrane (m/d),  $k_{dm}$  is the detachment rate of the EPS (/d), and  $m$  is the EPS density on the membrane surface (kg/m<sup>2</sup>).

$k_{dm}$  can be further expressed as:

$$k_{dm} = \eta(\tau_m - \Delta_m \Delta P) \quad (4)$$

where  $\eta$  is constant (1/d-Pa),  $\tau_m$  is the shear stress (Pa),  $\Delta_m$  is the coefficient of static friction, and  $\Delta P$  is the transmembrane pressure (Pa).

The shear stress ( $\tau_m$ ) due to EPS [31], can be further expressed as:

$$\tau_m = \rho_t g \delta \quad (5)$$

Where  $\rho_t$  is the density of mixed liquor for a known concentration of  $x$ , which can be obtained by the expression given by Busch et al. [52].  $\delta$  is the thickness of EPS biofilm (m).

### 2.5.3. SMP concentration in the bioreactor

To explore the effects of pore blocking in the HBSAnMBR during (Phase 1a, 1b, 2a, 2b, 3–5), Equations (9) and (10) given by Charfi et al. [47] were used.

$$\frac{d\varepsilon}{dt} = -k_e \frac{Q_p}{A} \sigma [SMP] \varepsilon \quad (6)$$

Where  $Q_p$  is the permeate flowrate in m<sup>3</sup>/s,  $k_e$  is the coefficient of deposit porosity decrease,  $A$  is the membrane surface area in m<sup>2</sup>,  $\sigma$  is the SMP fraction retained by the membrane, SMP concentration is expressed in kg/m<sup>3</sup>, and  $\varepsilon$  is the deposit pore diameter of the membrane. Charfi et al. [47] also gave a relationship between  $E$  and  $\varepsilon$  as:

$$E = \frac{\varepsilon}{\varepsilon + n} \quad (7)$$

Where  $E$  is the negative correction parameter, and  $n$  is equal to 1.

### 2.5.4. Dynamics of fouling in HBSAnMBR

The dynamics of the fouling process due to cake formation were examined from the extracted EPS containing proteins and carbohydrates, while a dynamic fouling model [42] was used to explore the fouling propensities and is given as follows:

$$v \frac{dM_{jc}}{dt} = J_{j2} \alpha \frac{M_{jc}}{R_c} + J_{j4} \alpha \frac{M_{jc}}{R_c} \quad (8)$$

According to Olubukola et al. [42],  $J_{j2}$  is defined as the flux in contact with the area of the membrane  $A_1$  in g/d-m<sup>2</sup> and  $J_{j4}$  is the flux in g/d-m<sup>2</sup>, which is in contact with the area of membrane  $A_2$ . The quantity  $M_{jc}$  is the mass concentration of the cake foulant in g/L that resulted in the cake fouling,  $\alpha$  is the specific resistance of the cake (1/m),  $R_c$  is the cake resistance in (1/m).

Based on the derivation elucidated by Olubukola et al. [42], the coefficient of fouling formation can be represented as 'a' and 'b' with this expression depicted by their corresponding values as:

$$\frac{J_{j2} \alpha}{R_c v} = a; \frac{J_{j4} \alpha}{R_c v} = b \quad (9)$$

Where  $v$  is the wet volume of the HBSAnMBR. If the area of the membrane is uniform i.e.,  $a = b$ , and  $a = \gamma$ ; then the total coefficient of fouling is represented as:

$$a + b = 2\gamma \quad (10)$$

### 2.5.5. Filtration resistance

The filtration resistance ( $R_t$ ) is the sum of membrane resistance, concentration polarization resistance, resistance due to the cake layer, and pore blocking. This can be expressed as;

$$R_t = R_p + R_c + R_m + R_{cp} \quad (11)$$

where  $R_t$  is the total filtration resistance (1/m),  $R_p$  is resistance due to pore blocking (1/m),  $R_c$  is resistance due to the cake layer (1/m),  $R_m$  is membrane resistance (1/m), and  $R_{cp}$  is concentration polarization resistance (1/m). Since the present study focuses only  $R_c$  and  $R_p$ ,  $R_{cp}$  was not taken into consideration in this study, so ( $R_t$ ) can be expressed as:

$$R_t = R_p + R_c + R_m \quad (12)$$

While the relation between TMP, viscosity ( $\mu$ ), flux ( $J$ ), and  $R_t$ , is given by:

$$J = \frac{\Delta P}{\mu R_t} \quad (13)$$

The viscosity of permeate ( $\mu$ ) was calculated using Equation (11) as given by Xing et al. [53]

$$\mu = \frac{0.33 * x + 2.3}{(1 + 0.0337 * T + 0.000221 * T * T) / 1000} \text{ (Pa.s)} \quad (14)$$

## 2.6. Statistical data analysis

A paired sample  $t$ -test was performed using the SPSS V.21 at a 95 % confidence interval (CI). Further, an analysis of variance (ANOVA) was also conducted in SPSS to validate the fitting results. The best curve-fitting results represent a higher correlation coefficient value ( $R^2$ ).

## 3. Results and discussion

### 3.1. Impact of organic loading rate (OLR) on biomass concentration during the operation phases

The applied OLR and biomass concentration are crucial parameters that determine the filterability and operational stability of the SANMBR. Past studies [54,55] reported that MLSS concentrations over 10 g/L lead to the entrapment of all particles larger than 20  $\mu$ m. The entrapped particles caused the solids to swell, increasing membrane resistance and system overload. The system overload reduces the ability of sludge to settle and reduces the overall treatment efficiency of SANMBR.

This study found that the MLSS and MLVSS concentrations correlated positively with OLR during Phases 1a, 1b, 2a, 2b, and 3–5, as shown in Figs. 2(a) and 2(b). On day 1, while commissioning the HBSAnMBR, the MLSS and MLVSS concentrations were 46.6 g/L and 39.18 g/L averaging 34.31 g/L and 29.12 g/L during Phase 1a, indicating that the HBSAnMBR mixed liquor was in a semi-solid state. Due to this, the OLR was intentionally kept as low as 1.05 kg-COD/m<sup>3</sup>/d at an HRT of 3.35 d. Using the numerical model developed previously for AnMBR (Equation (1)), the biomass concentration was simulated and fitted with experimental data, giving values of the coefficients; yield of biomass ( $Y = 0.13$  g-MLSS/g-COD) and decay of biomass ( $K_{dx} = 0.07$ /d) for Phase 1a, as shown in Fig. 2(b). The food-to-microorganism ratio (F/M) during Phase 1a was as low as 0.08 g-COD/g-MLSS. This could be attributed to low food availability leading to significant cell decay due to endogenous respiration [56]. These findings agreed with previous AnMBR studies [19,36,57]. In Phase 1b, the OLR was further increased to 1.45 kg-COD/m<sup>3</sup>/d, with an HRT of 2.90 d. The average MLSS and MLVSS concentrations during this period were 23.10 g/L and 18.65 g/L, respectively. As a result of the relative increase of OLR during Phase 1b, the F/M ratio and the biomass yield ( $Y$ ) increased to 0.13 g-COD/g-MLSS and 0.17 g-MLSS/g-COD, respectively. Conversely, the decay of cells ( $K_{dx}$ ) declined by 57 % from 0.07/d (Phase 1a) to 0.03/d (Phase 1b) due to the availability of sufficient food.

To mitigate fouling and frequent membrane cleaning due to the high-biomass concentration in the HBSAnMBR, Phases 2a and 2b were

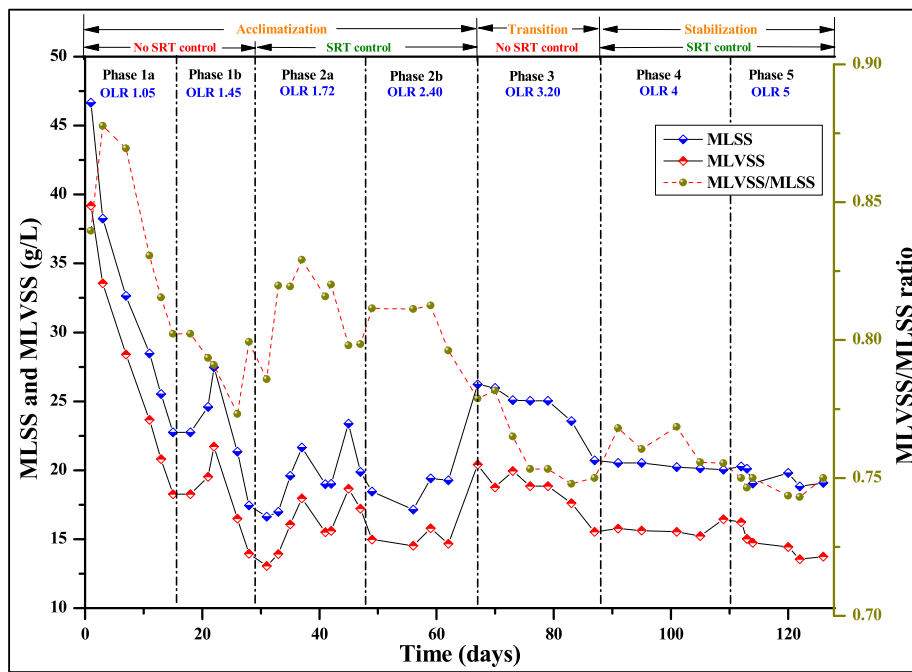


Fig. 2a. Variation of experimental MLSS, MLVSS concentration and MLVSS/MLSS ratio with time during different phases at OLR 1.05–5 Kg-COD/m<sup>3</sup>/d.

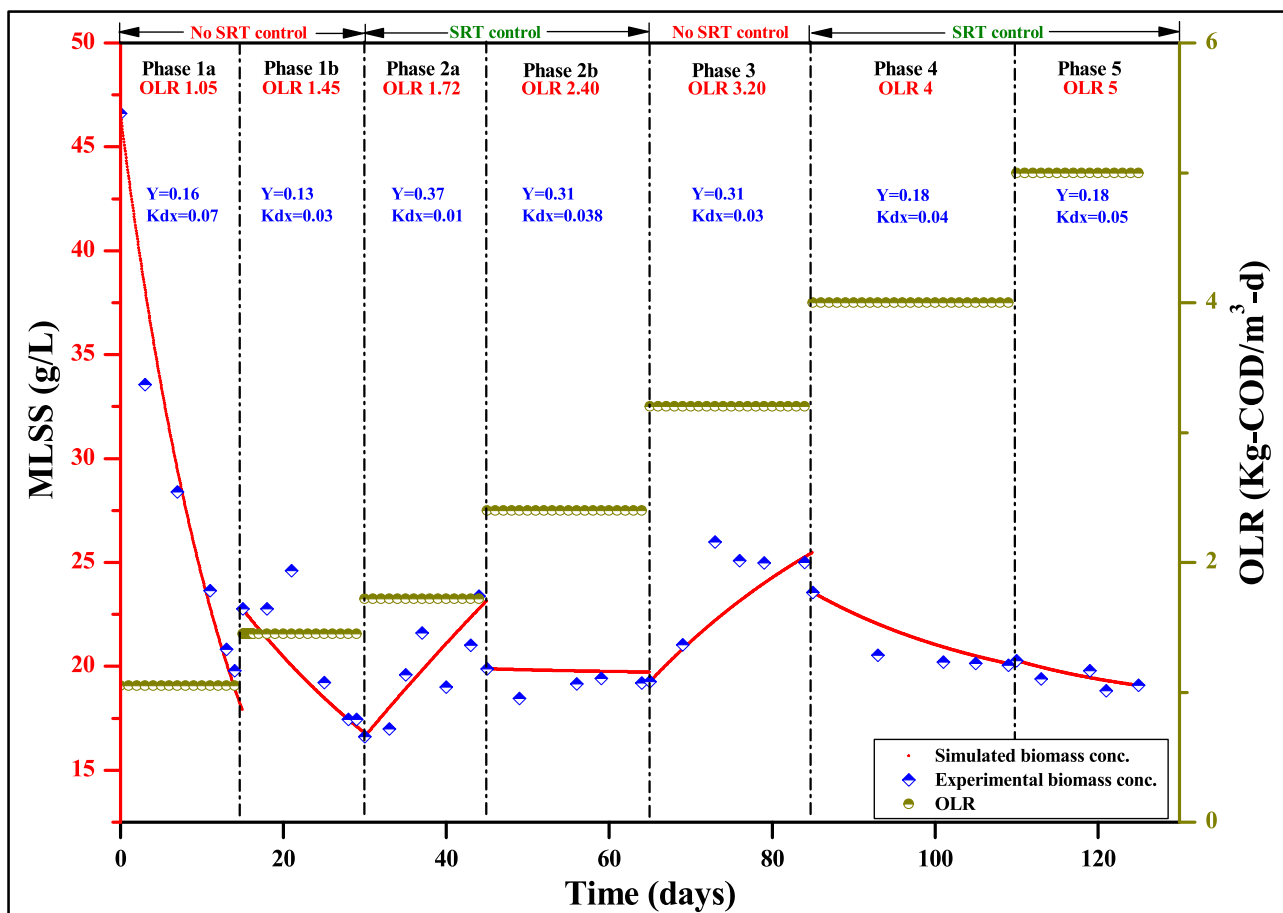


Fig. 2b. Variation of simulated and experimental MLSS concentration during different phases at OLR 1.05–5 kg-COD/m<sup>3</sup>/d.

operated under SRT control [58]. This was achieved by intentionally removing the sludge from the HBSAnMBR to maintain a biomass concentration of around 20 g/L. From the 30th day (Phase 2a) to the end of the 64th day (Phase 2b), the SRT was calculated at 20 and 10 days, respectively. After implementing SRT control,  $Y$  during Phases 2a and 2b increased to 0.37 and 0.31 g-MLSS/g-COD, respectively and correlated positively with the OLR increase (1.72 and 2.40) kg-COD/m<sup>3</sup>/d. Although the yield was high, the MLSS concentration stabilized around 19.46 and 18.72 g/L, respectively, as shown in Fig. 2(a) and 2(b)). During these phases (Phase 2a and 2b), the decay coefficient ( $K_{dx}$ ) was found to be 0.01 and 0.038/d, respectively, which attributed to a much more stable operation with F/M ratios of 0.15 and 0.13 g-COD/g-MLSS respectively.

Phase 3 could be attributed to the transition phase towards stabilization as the HBSAnMBR started showing stable treatment performance in terms of operation and COD removal. The OLR during Phase 3 was further increased to 3.20 kg-COD/m<sup>3</sup>/d with an HRT of 1 day. Due to this, the HBSAnMBR experienced an increase in MLSS concentration by 30 % from Phase 2b, averaging 24.3 g/L, as shown in Fig. 2(b). However, due to a power outage at our PC-2 laboratories, the SRT control could not be implemented, and the bioreactor's sludge was not intentionally wasted except for sampling. This observation confirmed that controlling the SRT effectively maintained the biomass concentration in the HBSAnMBR during Phase 2a and 2b. The biomass yield ( $Y$ ) during Phase 3 was found insignificant and was almost similar to Phase 2b (0.31 g-MLSS/g-COD), even though the OLR was increased to 3.20 kg-COD/m<sup>3</sup>/d, as shown in Table 4. This phase could be attributed to the transition from the log phase to the stationary phase, as it does not increase the biomass yield in multiples but keeps it static, even at a high F/M ratio (0.13 g-COD/g-MLSS).

Phases 4 and 5 were operated with SRT of 14 and 10 days, respectively, and the HBSAnMBR showed optimum performance during these phases. During these Phases, the HRT reduced significantly to 0.83 and 0.69 days, respectively, with an increase in the OLR. Although the OLR was increased to 4 kg-COD/m<sup>3</sup>/d (Phase 4) and 5 kg-COD/m<sup>3</sup>/d (Phase 5), the MLSS concentrations stabilized around 20 g/L. The SRT control was proven effective in attaining a sustainable biomass concentration in the HBSAnMBR for its stable operation and performance. The increased OLR during Phases 4 and 5 correlated positively with the F/M ratio (0.18 and 0.26 g-COD/g-MLSS) and the yield (0.18 g-MLSS/g-COD), respectively. These findings strongly agreed with past AnMBR studies [59,60]. In summary, the biomass concentration and yield correlated positively with the OLR. At the same time, a low OLR resulted in a low F/M ratio leading to substantial death of microorganisms ( $K_{dx}$ ) due to competition.

### 3.2. Dynamics of production of polymeric substances in the HBSAnMBR

To predict the influence of foulants dynamics on the performance of the HBSAnMBR process, the EPSc dynamics were simulated using Equation (8). As shown in Fig. 3a–3g, the EPSc (carbohydrate) and EPSp (protein) concentrations fit with the experimental data. The measured and simulated concentrations of EPSp were higher than EPSc. It was noticed that 140 mg/L of EPSp formed during Phase 1 was higher than the 60 mg/L of EPSc formed during the same phase. These values kept fluctuating at different stages. During all phases, the concentration of

EPSp was higher than EPSc. The model estimated parameters are depicted in Table 4. The formation of EPS significantly affected the performance of HBSAnMBR, while operating parameters such as OLR influence the EPS yield and decay rate. Within the OLR 1.05 kg-COD/m<sup>3</sup>/d, it was observed that the yield of EPSc was 0.00005 g-EPS/g-MLSS, and that of EPSp was 0.00008 g-EPS/g-MLSS. As the organic loading rate increases, a reasonable decrease in the yield of EPSc and that of EPSp is observed, as shown in Table 4.

The decay rate of EPSc and EPSp are other essential parameters upon which the performance of HBSAnMBR depends [31]. With the EPS formation during Phase 1a, the decay rate was observed to be 0.002/d and 0.002/d for EPSc and EPSp at OLR 1.05 kg-COD/m<sup>3</sup>/d, respectively. As the organic loading rate increases in the subsequent phases, the decay rate significantly increases at different organic loading rates, as shown in Table 4. Phases 3 and 4 were noticeable for a drastic increase, observed at 0.01/d and 0.07/d, respectively. This observation supports an assertion by Olubukola et al. [42] that the dynamics of EPSc and EPSp formation are critical factors responsible for the performance of SanMBR. Being able to control these dynamics would lead to improved membrane performance due to the reduction in the coefficient ( $\gamma$ ) responsible for fouling formation. With an increase in OLR during Phase 5, the EPSc and EPSp decay rates were significantly decreased.

The time-based variation of SMP formation is illustrated in Fig. 4(a). In Phase 1a, the formation of SMPp was 67 % more than SMPc. When the SMPp during Phase 1a was compared with SMPp during Phase 1b, there was a recorded increase of 35 %. During the long-term HBSAnMBR operation across all phases, SMPp formation was higher than SMPc. Compared to the previous phases, a moderate and constant rate of increase in SMPp and SMPc was observed during Phases 4 and 5. According to Balçoğlu et al. [20], protein concentration in the SMP and EPS is higher than that of carbohydrates. This result can be explained due to slow protein hydrolysis compared to carbohydrate hydrolysis, protein adsorption due to electrostatic interaction force which dominates protein adsorption on the membrane surface, and high colloidal stability that minimizes protein adsorption on the membrane surface leading to reduced protein concentration [69]. In summary, the EPS, SMP dynamics, and yield significantly impacted the fouling rate and HBSAnMBR performance.

#### 3.2.1. Influence of SMP on membrane pore blocking

The model proposed in Equation (6) simulates the impact of SMP on the membrane's pores diameter at 2 %, 5 %, and 10 % SMP entrapment, as given by Charfi et al. [47]. The simulated results are illustrated in Fig. 4(b). A consequential reduction of the pores was observed due to the entrapment of SMP within the cake layer; as the decay rate of SMP reduces, the amount of SMP available for the entrapment increases, as shown in Fig. 4(b). The entrapment process changed intermittently within Phases 1a, 1b, 2a, 2b, and 3 at given SMP concentrations. In Phases 4 and 5, the concentration of SMP became almost stable, and there was no significant influence of SMP concentration on the pore-blocking at all entrapment rates (2 %, 5 %, and 10 %), as shown in Fig. 4(b). With 10 % SMP entrapment, the porosity reduction was negligible in Phases 4 and 5. As most of the pore-blocking necessitated by SMPs was removed by ordinary backwashing, the findings of this study validated the effectiveness of backwashing in mitigating

**Table 4**  
Model estimated parameters for the current study.

Parameters	Description	Unit	Phase 1a	Phase 1b	Phase 2a	Phase 2b	Phase 3	Phase 4	Phase 5
$Y$	Yield coefficient of biomass	g-MLSS/g-COD	0.13	0.17	0.37	0.31	0.31	0.18	0.18
$K_{dx}$	Biomass decay rate	/day	0.07	0.03	0.01	0.03	0.03	0.04	0.05
$\beta_1$ (Carbohydrate)	Yield of EPSc	g-EPSc/g-MLSS	0.00005	0.00003	0.00001	0.00002	0.000013	0.00001	0.00001
$\beta_{dp1}$ (Carbohydrate)	EPSc decay rate	/d	0.002	0.003	0.04	0.0012	0.01	0.07	0.0012
$\beta_2$ (Protein)	Yield of EPSp	g-EPSp/g-MLSS	0.00008	0.00005	0.00003	0.00003	0.00001	0.00001	0.00001
$\beta_{dp2}$ (Protein)	EPSp decay rate	/d	0.002	0.003	0.0004	0.0012	0.000012	0.01	0.000002
$\gamma$	Coefficient of EPS fouling	/d	0.0005	0.00003	0.000016	0.00015	0.00025	0.000002	0.000002

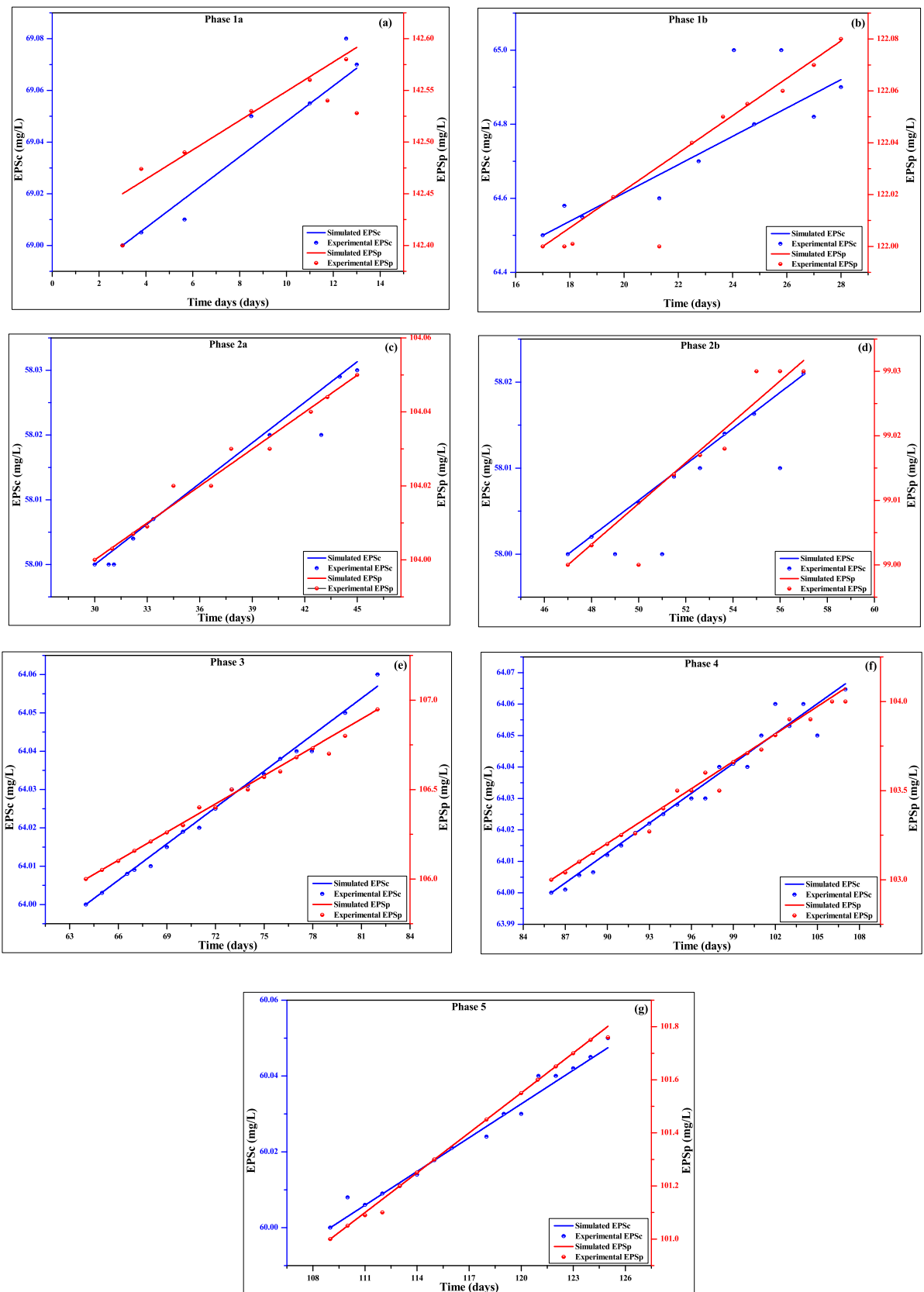


Fig. 3. (a), (b), (c), (d), (e), (f), and (g): Simulated and experimental EPSc and EPSp concentration for Phases 1a, 1b, 2a, 2b, and 3–5.

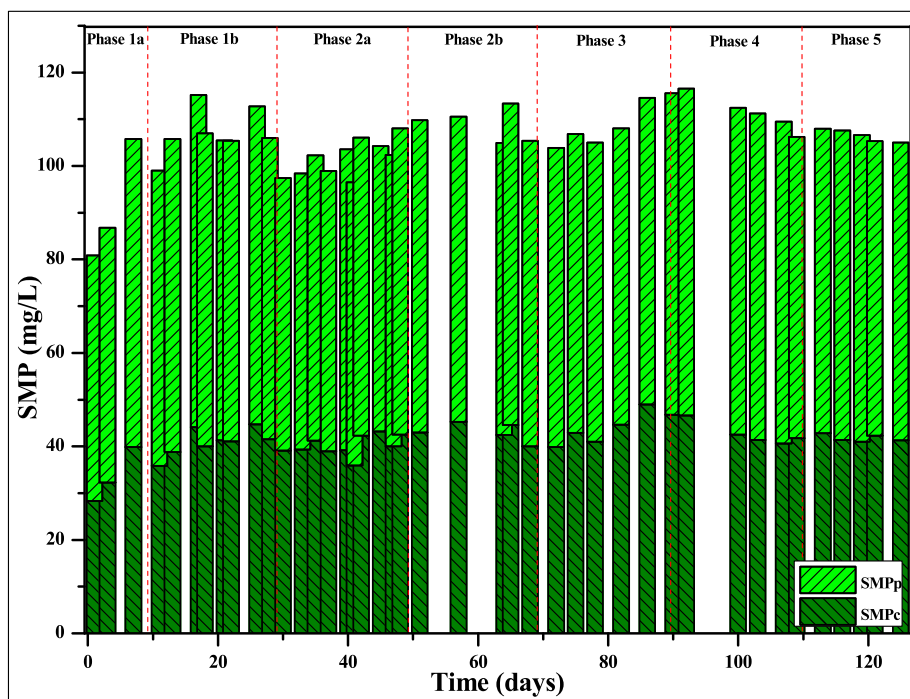


Fig. 4a. Variation of SMP during various phases of HBSAnMBR operation.

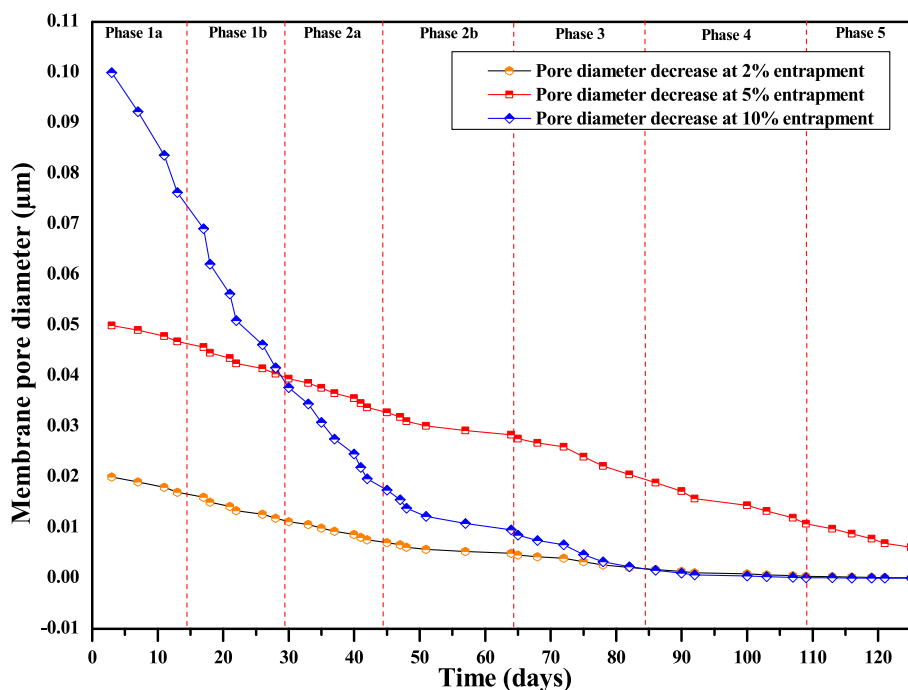


Fig. 4b. Simulated decrease in the membrane pore diameter ( $\mu\text{m}$ ) of ceramic UF membrane at 2 %, 5%, and 10 % of SMP entrapment.

membrane fouling due to pore-blocking in ceramic UF membranes. Compared with the performances of the AnMBR-coupled polymeric membranes reported in previous studies [22,26], the ceramic UF membrane used in this study demonstrated anti-fouling properties and sustainable membrane operation at high biomass and high organic loading rates.

### 3.3. Filtration performance

The filtration performance improved as the membrane flux increased

to 4.5 and 7.5 LMH with SRT control during Phases 2a and 2b, respectively. When the membrane flux values were compared with previous phases (Phases 1a and 1b), and those after the SRT control (Phases 2a and 2b), the average membrane flux values (4.75 and 7.5 LMH) with the SRT control were higher than those (3 and 3.6 LMH) without the SRT control, as shown in Table 2. As the filtration processes continued, the fouling coefficient ( $\gamma$ ) decreased. During Phase 1a, there was a slight increase in EPSc from 69.0 mg/L until it reached 69.09 mg/L, with the coefficient of fouling ( $\gamma$ ) estimated to be 0.00005/d, as shown in Fig. 3 (a) and Table 4. As the OLR increases in the subsequent phase (Phase

1b), a decrease in the concentration of both EPSc and EPSp is observed, as illustrated in Fig. 3(b). The EPSc and EPSp in Phase 1b were estimated to decrease by 7.2 % and 14.4 %, respectively, compared to Phase 1a.

With the implementation of SRT control in Phase 2a, the EPSc and EPSp concentrations decreased by 9.4 % and 18.9 %, respectively, as shown in Fig. 3(c). Despite the reduction in the  $\gamma$  coefficient, a sharp increase in EPSc and EPSp concentrations was observed during Phase 2b, as shown in Fig. 3(d). In Phase 3, no noticeable change in  $\gamma$  was observed, as shown in Fig. 3(e). This result supported the claim made by Olubukola et al. [42] that the fouling propensity of the membrane in AnMBR is due to an array of factors, including OLR, during the long-term operation. Due to an increase in OLR during Phases 4 and 5, a more than 9 % reduction in EPSc and EPSp was observed, as shown in Fig. 3(f) and 3(g), with a noticeable drop in the  $\gamma$ , as shown in Table 4. During these phases, the filtration process was significantly optimized, which reduced the possibility of fouling formation. The claim by some of the previous AnMBR studies conducted by Balcioglu et al. [20,31,42] confirms that membrane fouling depends on OLR and other operating parameters, such as yield of the biomass, concentrations of EPS and SMP, and microbial activities, supported the findings of this study.

As shown in Fig. 5, the TMP was relatively high during Phase 1a, i.e., above 70 kPa after 3 days of HBSAnMBR operation. This could be attributed to a high biomass concentration in the SANMBR (around 40 g/L) and a semi-solid state of biomass, leading to the rapid formation of the cake layer. To mitigate this issue, chemical cleaning of the membrane was conducted on the third day and at the end of Phase 1a, which brought the TMP to 15 kPa. With an increase of OLR during Phase 1b, the TMP increased and reached around 68 kPa by the end of Phase 1b, as shown in Fig. 5, and the membrane required chemical cleaning.

SRT control was initiated in Phase 2a to reduce the biomass concentration and mitigate frequent membrane cleaning. Further TMP analysis during Phase 2a shows a significant increase in TMP, i.e., above 65 kPa on the 35th day of HBSAnMBR operation. Chemical cleaning of the membrane was conducted due to a heavy cake layer build-up, as the MLSS concentration was still around 23 g/L during this period. SRT control during Phase 2b brought the MLSS concentration to around 20 g/L. SRT control could not be implemented in Phase 3 due to a power outage, and the sludge was not intentionally removed except for sampling. However, the OLR was increased to 3.2 kg-COD/m<sup>3</sup>/d, which increased MLSS concentration to 24.3 g/L. The TMP reached around

60–65 kPa during Phase 3, and chemical cleaning was conducted on the 72nd day of operation. During Phase 4, the OLR was increased to 4 kg-COD/m<sup>3</sup>/d, and SRT control was implemented. The TMP during this period was recorded as reasonably low, swinging between 26 and 32 kPa.

During Phase 5, the OLR was further increased to 5 kg-COD/m<sup>3</sup>/d, which was the highest OLR for this study, leading to an increased TMP of around 40–45 kPa. From the results, it can be concluded that the HBSAnMBR showed optimum performance during Phase 4 at a stable TMP range, stable biomass yield, increased EPS decay rate, reduced  $\gamma$  coefficient, and high permeate flux at OLR 4 kg-COD/m<sup>3</sup>/d. The total resistance during Phases 1a, 1b and 2a were higher than in the other phases, as depicted in Fig. 5. While during phase 2b, the total resistance reduced to  $1 \times 10^{10}$  (1/m) and remained stable in later phases, as shown in Fig. 5.

### 3.4. Membrane fouling characterization

SEM-EDX and FTIR spectroscopy was used to conduct autopsy analyses of the ceramic UF membrane used in this study and the cake layer collected from the surface of the membrane during different phases of the experiment. The membrane surface was analyzed before (clean membrane) and after the formation of the cake layer (fouled membrane), as shown in Fig. 6(a), (b) and (c) to elucidate the fouling mechanism. In contrast, the collected cake layer's morphology and chemical composition during Phases 1a, 1b, and 3 were thoroughly investigated using SEM-EDX and ATR-FTIR spectroscopy (Fig. 7(b), (c), and (d)). The cake layer formation was insignificant during Phases 4 and 5 due to stable HBSAnMBR operation and less fouling.

The SEM images of the clean membrane (Fig. 6(a)) show a smooth surface free of particles that could trap inorganic colloids, macromolecules, and microbial flocs. On the other hand, the fouled membrane exhibited a relatively rough surface and appeared to contain bacteria, EPS floc, and particles, as shown in Fig. 6(a). It was assumed that the hydrophobic nature of EPS expedited the production of the cake layer on the membrane surface [20], as the cake layer was primarily composed of EPS. A high protein concentration in the EPS (EPSp) was found, and it was assumed that the interaction between the membrane surface and protein prevented the foulants from being entirely eliminated from the membrane surface. The membrane pores were clearly visible in the

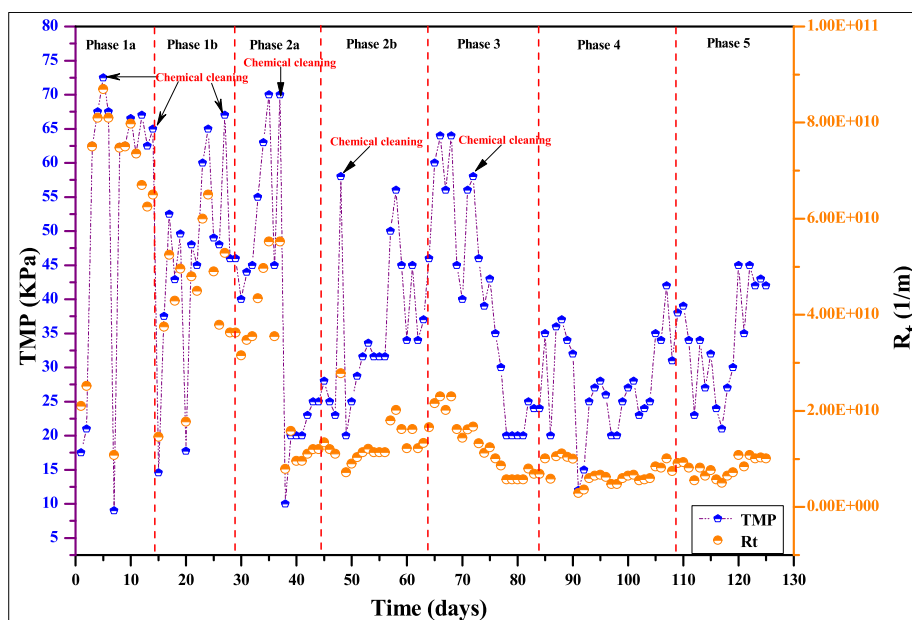


Fig. 5. Variation of transmembrane pressure (TMP) and total filtration resistance ( $R_t$ ) during different phases of HBSAnMBR operation.

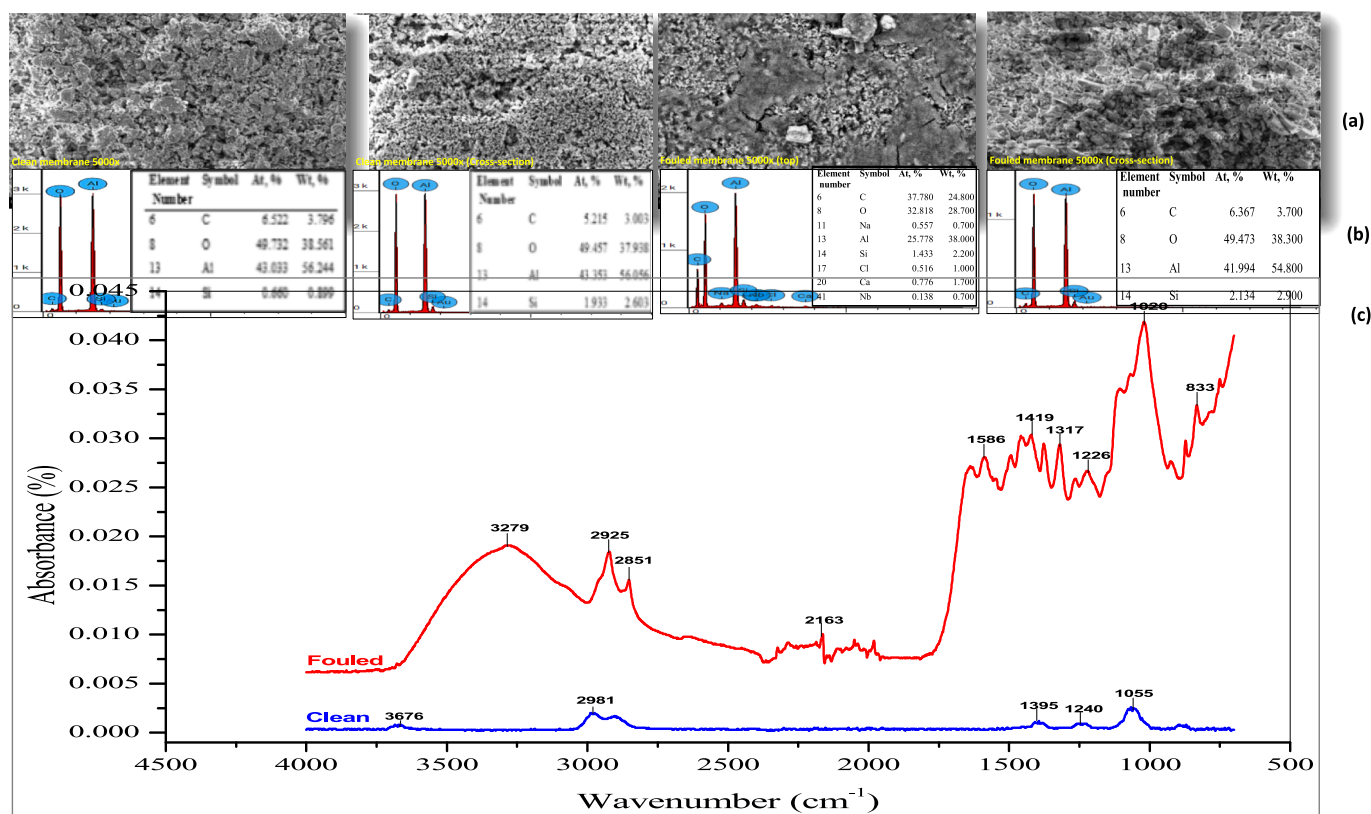


Fig. 6. Membrane morphology of clean and fouled membrane: (a) SEM imaging (top and cross-section view), (b) EDX analyses, (c) FTIR analyses.

cross-section of the clean and fouled membranes, as shown in Fig. 6(a), indicating that membrane pores did not experience pore blockage, while cake layer formation was found to be a critical fouling mechanism. The cake layer was collected from the membrane surface during Phases 1a, 1b and 3 for analysis and was found to be compact, dense, and evenly distributed, as seen in Fig. 7(a) and 7(b). It was found that at high biomass concentrations, removing the cake layer was quite impossible using normal backwashing.

The EDX analysis revealed that inorganic foulants on the clean membrane surface correlated with the foulant composition on the fouled membrane surface, which included Al (43.03 and 25.77 %), and Si (0.66 and 4.43 %), respectively. Additionally, the presence of calcium (0.77 %) and sodium (0.55 %) on the fouled membrane (Fig. 6(b)) may have contributed to the inorganic fouling [61]. The high concentration of Al was due to the fingerprint of the membrane (Al<sub>2</sub>O<sub>3</sub>). The results of EDX demonstrated that foulants accumulated on the membrane were primarily organic and could be distinguished from the carbon (37.7 %) and oxygen (32.81 %) peaks, as shown in (Fig. 6(b)).

The collected cake layer was analyzed using EDX during Phases 1a, 1b and 3, and it found that the cake layer was primarily composed of elements: C, O, Na, Mg, Al, Si, P, F, Ca, and Mo, as shown in Fig. 7(c). Although during Phases 1a, 1b and 3, the relative content of Al (1.41, 0.61 and 0.87 %), Si (0.6, 0, and 0.58 %), Na (0.49, 0.64 and 0.7 %), Mg (0.4, 0, 0 %), was low, these elements had a significant impact on the formation of the membrane cake layer [61]. A notably high concentration of Phosphorous (5.89 %) was detected during Phase 1b. A trace amount of Molybdenum (Mo) (0.29 and 0.3 %) was also found in the cake layer during Phases 1a and 3, respectively, which could be a component of micro-nutrients added to the simulated abattoir wastewater. Khan et al. [60] reported a significant concentration of Mo attributed to wastewater component discharges from automotive industries in their fouling study. Furthermore, Khan et al. [62] also reported that the rare earth metals, which include Niobium and Molybdenum, minimize polar interaction leading to increasing

hydrophobicity in the membrane. In this study, we discovered that the interaction between Niobium and Molybdenum with ceramic UF membrane improved the fouling performance by reducing the SMP entrapment.

FTIR analysis was conducted to validate the membrane surface chemistry changes over time and to identify the cake layer's functional groups. Fig. 6(c) shows the clean and fouled ceramic UF membrane's FTIR spectra. Each peak demonstrates a particular type of molecular vibration; (symmetrical, asymmetrical, twisting, wagging, bending, deformation, or rocking), and some characterize the ceramic UF membrane skeleton (O-H group). The clean membrane's absorbance peaks at 3676, 2981, 1395, 1240 and 1055/cm are attributed to the ceramic membrane fingerprint [63]. As shown in Fig. 6(c), an intense peak around 3400/cm corresponded to (O-H) stretching vibrations of carboxylic acids and (N-H) stretching vibrations of amide or amine groups [64], around 2900 (C-H) stretching, about 1390 (C-H<sub>3</sub>) bending, 1250–1050 (C-O-C) stretch, and 950–1100 /cm (Si-O) stretching of silicates [65].

The spectra demonstrate a significant absorption (3200–3300/cm) in the fouled membrane (Fig. 6(c)) and the cake layer foulants (Fig. 7(d)) collected during Phases 1a, 1b and 3, which are caused by stretching the O-H bond in hydroxyl functional groups (phenols and/or alcohols). Around 2925/cm (Fig. 7(d)), the C-H stretch of alkanes may be seen, which could be attributed to carbohydrates [66]. Absorbance peak around 2164/cm in the fouled membrane (Fig. 6(c)) and the cake-layer foulants (Fig. 7(d)) could be attributed to (C≡C) stretch. The absorption bands detected around 1600/cm on the membrane surface (Fig. 6(c)), attributed to aromatic compounds and overlap with the absorption band of amides, while the fingerprints of amides I and II spectra, located around (1500–1600/cm) in the cake-layer foulants (Fig. 7(d)), correlate to the protein secondary structure [67]. This finding indicates the presence of proteins in the foulant cake layer. The (C-H) bend absorption band of alkanes around 1419/cm overlaps the absorption band of inorganic compounds (Fig. 6(c)), while the peak of around 1020/cm

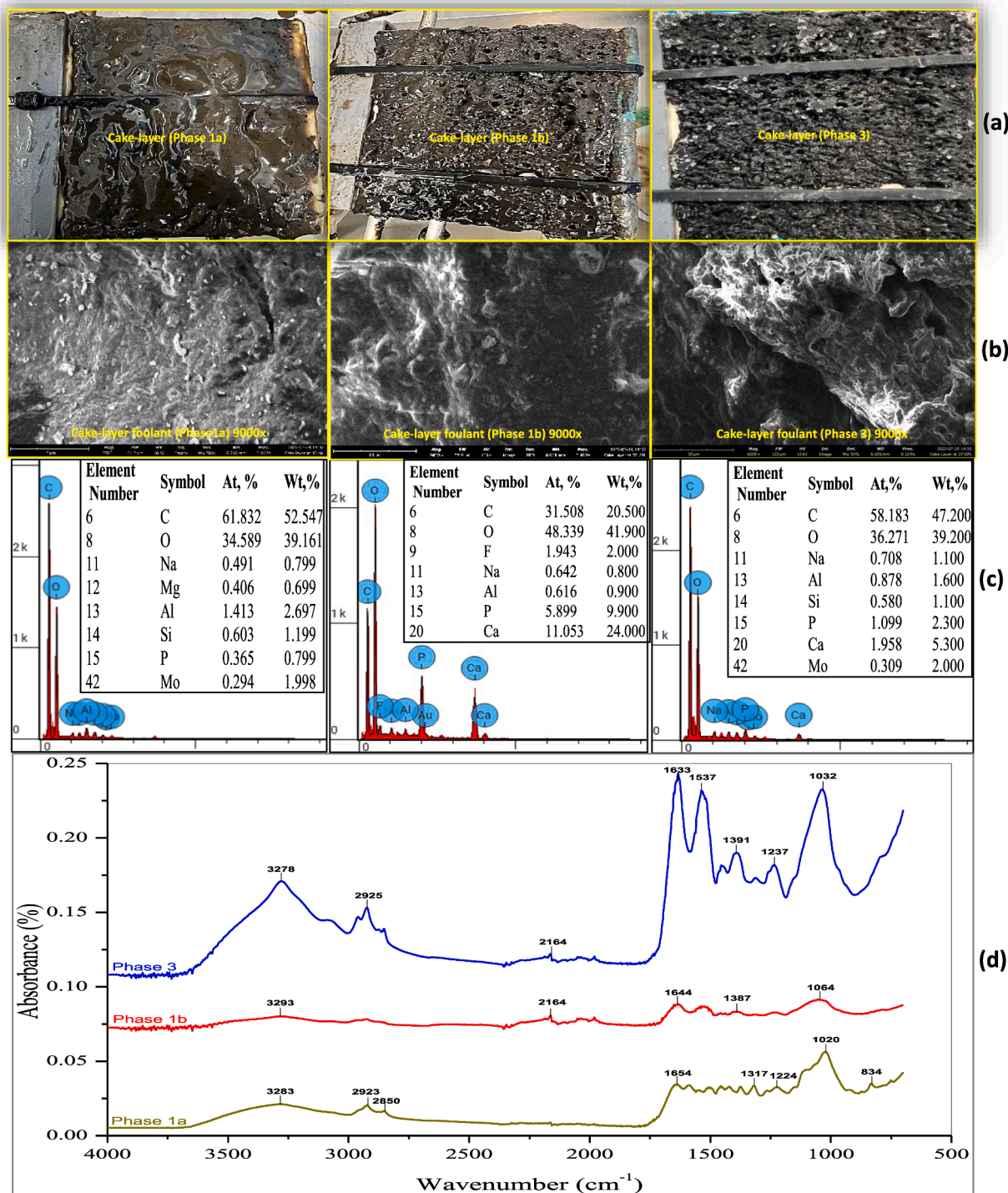


Fig. 7. Fouling morphology: (a) Cake-layer photographs, (b) SEM imaging of foulants, (c) EDX analyses, (d) FTIR analyses.

indicates the presence of polysaccharides or polysaccharide-like compounds. Broad absorption regions at about 1300/cm and a peak at 834/cm, as shown in Fig. 6(c) and Fig. 7(d), indicate the presence of carbonate and signs of  $\text{CaCO}_3$  scaling [68] due to the calcium-rich feed.

In conclusion, it was found that the formation of the membrane cake layer during Phases 1a and 1b increased the filtration resistance in the order of  $6.2 \times 10^{10}/\text{m}$  and  $4.83 \times 10^{10}/\text{m}$ , respectively. The EDX results of the fouled membrane indicated that membrane cake layer formation was the primary fouling mechanism, while sodium, phosphorous, and calcium triggered the inorganic fouling. The membrane pores did not

experience pore blockage. Within the technical information from this study, the non-polar interaction between the ceramic membrane and the inorganic foulants, as indicated by the EDX analysis in Fig. 6(b), improved the intrinsic hydrophobic property of the ceramic UF membrane. From the FTIR peaks (Fig. 6(c)), obtained from the fouled membrane surface (Fig. 6(c)) (3279, 2925, 1586, 1419, and 1020/cm) and the cake layer (Fig. 7(d)) (3278, 2925, 1633, 1537 and 1032/cm), it can be concluded that the cake layer foulants were primarily of organic origin.

### 3.5. Treatment performance of HBSAnMBR

The treatment performance of the HBSAnMBR system was assessed at various OLRs during Phases 1a, 1b, 2a, 2b, and 3–5 according to TP, TN, and COD removal efficiencies at 125 days of operation. The OLR values during Phases 1a, 1b, 2a, 2b, 3–5 were 1.05, 1.45, 1.72, 2.40, 3.2, 4 and 5 kg-COD/m<sup>3</sup>/d, respectively. Fig. 8 depicts how the influent COD loading affects COD removal effectiveness at various HRT. Past AnMBR studies [69,70] reported that a high MLSS concentration leads to a higher removal (%) for a specific COD-loaded effluent with increasing HRT. However, a poor treatment performance was observed in this study at a reportedly high MLSS concentration and high HRT during Phases 1a, 1b and 3, as shown in Fig. 8.

It was found that the permeate COD concentration increased with

increasing OLR during Phases 1a, 1b, and 3, and concentrations of 1622.62, 952.32, and 1020.94 mg/L were recorded at the end of Phases 1a, 1b and 3. During Phases 1a, 1b, and 3, the TP (20.22 %, 20.61 % and 19.81 %), TN (20.22 %, 20.61 % and 19.81 %) and COD (80.45 %, 88.53 % and 87.70 %) removal were recorded respectively. After implementing the SRT control in Phases 2a and 2b, the performance of HBSAnMBR improved as the OLR was increased to 1.72 and 2.40 kg-COD/m<sup>3</sup>/d, respectively. The COD removal was as high as 95.79 % and 95.66 %, respectively. During this period, the F/M increased to 0.15 and 0.13 g-COD/g-MLSS. A good treatment performance in terms of TP (23.59 and 26.32 %) and TN (41.43 and 40.78 %) removal efficiencies were observed during this period, as shown in Fig. 8. Power outage during Phase 3 led to poor performance. However, the OLR was increased to 3.2 kg-COD/m<sup>3</sup>/d during this period, maintaining an F/M ratio of 0.13

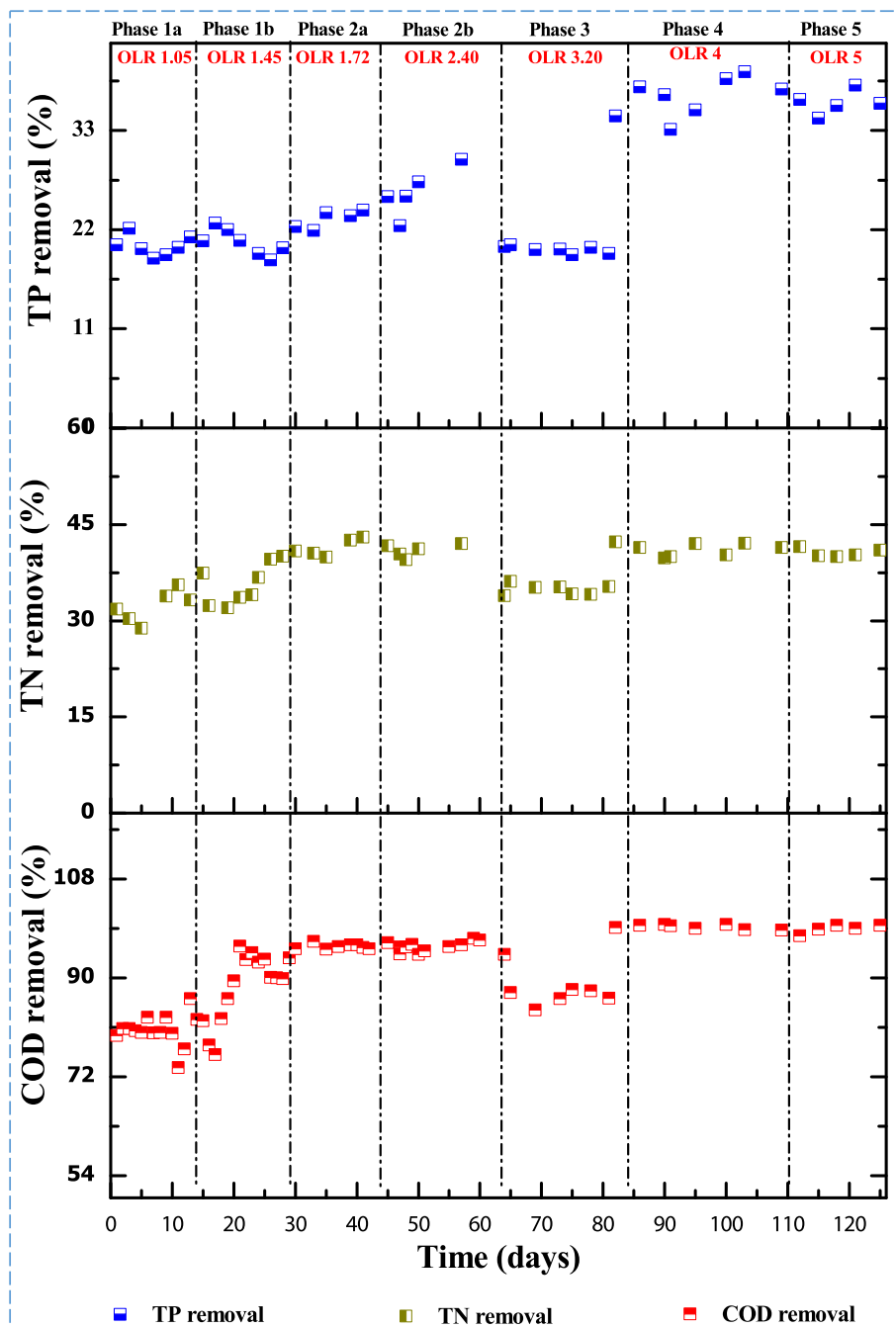


Fig. 8. Treatment performance of HBSAnMBR in terms of total phosphorous (TP), total nitrogen (TN) and chemical oxygen demand (COD) removal efficiencies during Phase 1a, 1b, 2a, 2b, and 3–5.

g-COD/g-MLSS. The TP, TN and COD removal efficiencies during Phase 3 were similar to Phase 1a and 1b, as shown in Fig. 8.

During Phase 4, at OLR 4 kg-COD/m<sup>3</sup>/d, a superior treatment performance was observed in terms of TP, TN, and COD removal of 36.58 %, 41.11 % and 99.33 %, respectively, at a high F/M and low HRT of 0.18 g-COD/g-MLSS and 0.83 days. This behaviour agreed with a past AnMBR study conducted by Inaba et al. [71] to treat organic solid waste under controlled and deteriorated conditions. Phase 5 was operated at a maximum OLR (5 kg-COD/m<sup>3</sup>/d) designed for this study. The removal efficiencies during this period were higher than Phases 1a, 1b, 2a, 2b, and 3 but lesser than Phase 4, as shown in Fig. 8. This indicates that the treatment performance of HBSAnMBR started to decline above OLR 4 kg-COD/m<sup>3</sup>/d.

In summary, the HBSAnMBR, when operated at low OLR and extremely high biomass concentration ( $18 \leq \text{MLSS (g/L)} \leq 35$ ) during the acclimatization and transition Phases (1a, 1b, 2a, 2b and 3), was able to remove COD over 80.45, 88.53, 95.79, 95.66 and 87.70 %, respectively. At OLRs (4 and 5 kg-COD/m<sup>3</sup>/d) and biomass concentration ( $19 \leq \text{MLSS (g/L)} \leq 25$ ), the HBSAnMBR consistently removed 99.33 and 98.88 % of COD. The present study was highly successful in meeting the trade-waste discharge limits (COD: 1500 mg/L; TP: 50 mg/L and TN: 150 mg/L) of the Australian water and wastewater association [72] by achieving high COD removal efficiencies (up to 99%).

### 3.6. Statistical analysis

Using SPSS software version 28.0.1, the model fitting results were verified. The correlation between simulated data and experimental results was analyzed at 95% CI (confidence intervals) using a paired sample *t*-test. The mean difference between two sets of observations (simulated and experimental) is typically calculated using a paired sample *t*-test [73]. According to Gupta and Kapoor [74], the two groups of data are regarded as “strongly correlated,” “moderately correlated,” and “least correlated” if their correlation coefficients lie between  $\pm 0.50$  to  $\pm 1.00$ ,  $\pm 0.30$  to  $\pm 0.49$  and less than  $\pm 0.29$  respectively. All estimated operating parameters: MLSS, EPS<sub>c</sub>, EPS<sub>p</sub>, TMP and filtration resistance, derived from model-fitted results with experimental data, were statistically correlated ( $p \leq 0.0137$ ), and the results are summarised in Table S2.

## 4. Conclusion

The HBSAnMBR was operated for 125 days to treat AWW at biomass concentrations of  $18 \leq \text{MLSS (g/L)} \leq 35$ . The treatment and operational performances at different OLR ranges of 1.05–5 kg-COD/m<sup>3</sup>/d were critically investigated during its long-term operation. The kinetic parameters governing biomass yield, production and decay of EPS, filtration resistance and decrease in membrane porosity due to SMP production during different phases were explored using numerical models, and their correlations were established. It was found that the OLR was a critical parameter responsible for the treatment performance and filtration performance of HBSAnMBR.

The key findings of this study are:

- At the OLR range (1.05–3.2) kg-COD/m<sup>3</sup>/d, the HBSAnMBR removed up to 95 % of COD, while a COD removal of 99.33 and 98.88 % was achieved at OLRs 4 and 5 kg-COD/m<sup>3</sup>/d, respectively.
- The biomass concentration (*x*) and yield (*Y*) correlated positively with the OLR and negatively correlated with the decay rate of microorganisms (*K<sub>dx</sub>*).
- The EPS<sub>p</sub> yield was significantly higher than that of EPS<sub>c</sub>, and the dynamic behaviour of EPS formation indicated a reasonable decrease of the fouling coefficient  $\gamma$  as the OLR increases, which accounts for favourable optimum performance at OLR 4 kg-COD/m<sup>3</sup>/d
- The HBSAnMBR had much pronounced organic fouling at high biomass concentrations ( $18 \leq \text{MLSS (g/L)} \leq 35$ ) without SRT control

during Phases 1a, 1b, and 3 at OLR (1.05, 1.45, and 3.2) kg-COD/m<sup>3</sup>/d, resulting in high cake resistance up to  $6.5 \times 10^{10}$ /m. At the same time, SRT control helped mitigate organic fouling during Phases 2a, 2b, 4, and 5 and achieved stable membrane operation at OLR (1.72, 2.40, 4 and 5) kg-COD/m<sup>3</sup>/d.

- The cake layer was primarily composed of polysaccharides and proteins. At the same time, Significant amounts of sodium, phosphorous and calcium depositions were detected in the cake layer deposited on the membrane's surface during high biomass concentrations, and their crystallization triggered inorganic fouling.
- The complex interaction between the rare earth metal like Molybdenum and Niobium provided better conditions to enhance the fouling performance of HBSAnMBR by improving the hydrophobicity of the ceramic membrane, which consequently reduced the entrapped SMP on the membrane pores.

The results highlighted that sustainable OLR was found as 4 kg-COD/m<sup>3</sup>/d, at which the HBSAnMBR exhibited superior treatment performance, less fouling and stable operational performance. With excellent operational and treatment efficiency, it is envisaged that this study will aid in developing a strategy for adopting SAnMBR as a pretreatment system to treat trade wastewater generated from abattoirs and similar high-strength industrial effluents. Further research is required to investigate the biomethane recovery performance and the associated microbial dynamics under extremely high-biomass concentration in a SAnMBR treating abattoir wastewater.

## Declaration of Competing Interest

The authors declare that they have no known competing financial interests or personal relationships that could have appeared to influence the work reported in this paper.

## Data availability

Data will be made available on request.

## Appendix A. Supplementary data

Supplementary data to this article can be found online at <https://doi.org/10.1016/j.cej.2023.142145>.

## References

- [1] B. McCabe, T. Schmidt, P. Harris, Crust management for optimal anaerobic digestion performance at meat processing facilities, Australian Meat Processing Corporation, North Sydney, NSW, Australia, 2017. Retrieved from: [Here].
- [2] P.D. Jensen, T. Sullivan, C. Carney, D. Batstone, Analysis of the potential to recover energy and nutrient resources from cattle slaughterhouses in Australia by employing anaerobic digestion, *Appl. Energy* 136 (2014) 23–31.
- [3] A.M.A. Pintor, V.J.P. Vilar, C.M.S. Botelho, R.A.R. Boaventura, Oil and grease removal from wastewaters: Sorption treatment as an alternative to state-of-the-art technologies. A critical review, *Chem. Eng. J.* 297 (2016) 229–255, <https://doi.org/10.1016/j.cej.2016.03.121>.
- [4] H.S. Abd El-Gawad, Oil and grease removal from industrial wastewater using new utility approach, *Adv. Environ. Chem.* 2014 (2014) 1–6.
- [5] I.A. Husain, M.F. Alkhatib, M.S. Jammi, M.E. Mirghani, Z. Bin Zainudin, A. Hoda, Problems, control, and treatment of fat, oil, and grease (FOG): a review, *J Oleo Sci* 63(8) (2014) 747–52. 10.5650/jos.ess13182.
- [6] Ö.B. Gökçek, S. Özdemir, Optimization of the coagulation–flocculation process for slaughterhouse wastewater using response surface methodology, *CLEAN–Soil, Air Water* 48 (7–8) (2020) 2000033.
- [7] P. Alfonso-Muniozuren, J. Lee, M. Bussemaker, R. Chadeesingh, C. Jones, D. Oakley, D. Saroj, A combined activated sludge-filtration-ozonation process for abattoir wastewater treatment, *Journal of Water, Process. Eng.* 25 (2018) 157–163, <https://doi.org/10.1016/j.jwpe.2018.07.009>.
- [8] K. Keerthana, R. Thivyatharsan, Constructed wetland for slaughterhouse wastewater treatment, (2018).
- [9] H.A. Aziz, N.N.A. Puat, M.Y. Alazaiza, Y.-T. Hung, Poultry slaughterhouse wastewater treatment using submerged fibers in an attached growth sequential batch reactor, *Int. J. Environ. Res. Public Health* 15 (8) (2018) 1734.

- [10] B.K. McCabe, I. Hamawand, P. Harris, C. Baillie, T. Yusaf, A case study for biogas generation from covered anaerobic ponds treating abattoir wastewater: Investigation of pond performance and potential biogas production, *Appl. Energy* 114 (2014) 798–808, <https://doi.org/10.1016/j.apenergy.2013.10.020>.
- [11] P. Jensen, S. Yap, A. Boyle-Gotla, J. Janoschka, C. Carney, M. Pidou, D. Batstone, Anaerobic membrane bioreactors enable high rate treatment of slaughterhouse wastewater, *Biochem. Eng. J.* 97 (2015) 132–141.
- [12] S. Sayed, L. van Campen, G. Lettinga, Anaerobic treatment of slaughterhouse waste using a granular sludge UASB reactor, *Biol. Wastes* 21 (1) (1987) 11–28.
- [13] Z. Zeng, P. Zheng, M. Zhang, A. Ghulam, Performance and working mechanism of a novel anaerobic self-flotation reactor for treating wastewater with high suspended solids, *Environ. Sci. Pollut. Res.* 26 (25) (2019) 26193–26202.
- [14] M. Atasoy, O. Eyice, Z. Cetecioglu, A comprehensive study of volatile fatty acids production from batch reactor to anaerobic sequencing batch reactor by using cheese processing wastewater, *Bioresour. Technol.* 311 (2020), 123529.
- [15] P.L. Lau, A.P. Trzcinski, A review of modified and hybrid anaerobic baffled reactors for industrial wastewater treatment, *Water Sci. Eng.* 15 (3) (2022) 247–256.
- [16] Y. Yao, Z. Gan, Z. Zhou, Y.-X. Huang, F. Meng, Carbon sources driven supernatant micro-particles differentiate in submerged anaerobic membrane bioreactors (AnMBRs), *Chem. Eng. J.* 430 (2022), 133020, <https://doi.org/10.1016/j.cej.2021.133020>.
- [17] C. Shin, S.H. Tilmans, F. Chen, C.S. Criddle, Anaerobic membrane bioreactor model for design and prediction of domestic wastewater treatment process performance, *Chem. Eng. J.* 426 (2021), 131912, <https://doi.org/10.1016/j.cej.2021.131912>.
- [18] Y. He, P. Xu, C. Li, B. Zhang, High-concentration food wastewater treatment by an anaerobic membrane bioreactor, *Water Res* 39 (17) (2005) 4110–4118, <https://doi.org/10.1016/j.watres.2005.07.030>.
- [19] R.K. Gautam, R. Valente, H. Abbas, A. Bui, N. More, S. Gray, S. Muthukumar, D. Navaratna, Recovery of biomethane from a submerged anaerobic membrane bioreactor treating domestic wastewater blended with semi-solid organic wastes discharged from residential establishments, *Environ. Technol. Innov.* 27 (2022), 102763, <https://doi.org/10.1016/j.eti.2022.102763>.
- [20] G. Balcioglu, G. Yilmaz, Z.B. Gonder, Evaluation of anaerobic membrane bioreactor (AnMBR) treating confectionery wastewater at long-term operation under different organic loading rates: Performance and membrane fouling, *Chem. Eng. J.* 404 (2021), 126261, <https://doi.org/10.1016/j.cej.2020.126261>.
- [21] H. Chen, S. Chang, Q. Guo, Y. Hong, P. Wu, Brewery wastewater treatment using an anaerobic membrane bioreactor, *Biochem. Eng. J.* 105 (2016) 321–331.
- [22] R. Lutze, M. Engelhart, Comparison of CSTR and AnMBR for anaerobic digestion of WAS and lipid-rich flotation sludge from the dairy industry, *Water Resour. Ind.* 23 (2020), 100122.
- [23] S. Chairapat, A. Thongsai, B. Charnnok, W. Khongnakorn, J. Bae, Influences of liquid, solid, and gas media circulation in anaerobic membrane bioreactor (AnMBR) as a post treatment alternative of aerobic system in seafood industry, *J. Membr. Sci.* 509 (2016) 116–124.
- [24] M. Turker, R.K. Dereli, Long term performance of a pilot scale anaerobic membrane bioreactor treating beet molasses based industrial wastewater, *J. Environ. Manage.* 278 (2021), 111403.
- [25] H. Wu, R. Dalke, J. Mai, M. Holtzapfel, M. Urgan-Demirtas, Arrested methanogenesis digestion of high-strength cheese whey and brewery wastewater with carboxylic acid production, *Bioresour. Technol.* 332 (2021), 125044.
- [26] N. Basset, E. Santos, J. Dosta, J. Mata-Álvarez, Start-up and operation of an AnMBR for winery wastewater treatment, *Ecol. Eng.* 86 (2016) 279–289.
- [27] S.I. Padmasiri, J. Zhang, M. Fitch, B. Norddahl, E. Morgenroth, L. Raskin, Methanogenic population dynamics and performance of an anaerobic membrane bioreactor (AnMBR) treating swine manure under high shear conditions, *Water Res.* 41 (1) (2007) 134–144.
- [28] H. Cheng, Y. Li, L. Li, R. Chen, Y.-Y. Li, Long-term operation performance and fouling behavior of a high-solid anaerobic membrane bioreactor in treating food waste, *Chem. Eng. J.* (2020), 124918, <https://doi.org/10.1016/j.cej.2020.124918>.
- [29] Z. Chen, X. Li, D. Hu, Y. Cui, F. Gu, F. Jia, T. Xiao, H. Su, J. Xu, H. Wang, P. Wu, Y. Zhang, N. Jiang, Performance and methane fermentation characteristics of a pilot scale anaerobic membrane bioreactor (AnMBR) for treating pharmaceutical wastewater containing m-cresol (MC) and iso-propyl alcohol (IPA), *Chemosphere* 206 (2018) 750–758, <https://doi.org/10.1016/j.chemosphere.2018.05.008>.
- [30] A. Plevri, D. Mamais, C. Noutsopoulos, Anaerobic MBR technology for treating municipal wastewater at ambient temperatures, *Chemosphere* 275 (2021), 129961, <https://doi.org/10.1016/j.chemosphere.2021.129961>.
- [31] R.K. Gautam, T. Kamilya, S. Verma, S. Muthukumar, V. Jegatheesan, D. Navaratna, Evaluation of membrane cake fouling mechanism to estimate design parameters of a submerged AnMBR treating high strength industrial wastewater, *J. Environ. Manage.* 301 (2022), 113867, <https://doi.org/10.1016/j.jenvman.2021.113867>.
- [32] H.J. Luna, B.E.L. Baeta, S.F. Aquino, M.S.R. Susa, EPS and SMP dynamics at different heights of a submerged anaerobic membrane bioreactor (SAMBR), *Process Biochem.* 49 (12) (2014) 2241–2248.
- [33] I. Martin-Garcia, V. Monsalvo, M. Pidou, P. Le-Clech, S. Judd, E. McAdam, B. Jefferson, Impact of membrane configuration on fouling in anaerobic membrane bioreactors, *J. Membr. Sci.* 382 (1–2) (2011) 41–49.
- [34] E. Maleki, A. Bokhary, K. Leung, B. Liao, Long-term performance of a submerged anaerobic membrane bioreactor treating malting wastewater at room temperature (23±1 °C), *J. Environ. Chem. Eng.* 7 (4) (2019), 103269.
- [35] A. Aslam, S.J. Khan, H.M.A. Shahzad, Impact of sludge recirculation ratios on the performance of anaerobic membrane bioreactor for wastewater treatment, *Bioresour Technol* 288 (2019), 121473, <https://doi.org/10.1016/j.biortech.2019.121473>.
- [36] A. Robles, M.V. Ruano, A. Charfi, G. Lesage, M. Heran, J. Harmand, A. Seco, J. P. Steyer, D.J. Batstone, J. Kim, J. Ferrer, A review on anaerobic membrane bioreactors (AnMBRs) focused on modelling and control aspects, *Bioresour Technol* 270 (2018) 612–626, <https://doi.org/10.1016/j.biortech.2018.09.049>.
- [37] D. Navaratna, L. Shu, K. Baskaran, V. Jegatheesan, Model development and parameter estimation for a hybrid submerged membrane bioreactor treating Ametryn, *Bioresour Technol* 113 (2012) 191–200, <https://doi.org/10.1016/j.biortech.2011.12.017>.
- [38] R. Chen, Y. Nie, Y. Hu, R. Miao, T. Utashiro, Q. Li, M. Xu, Y.-Y. Li, Fouling behaviour of soluble microbial products and extracellular polymeric substances in a submerged anaerobic membrane bioreactor treating low-strength wastewater at room temperature, *J. Membr. Sci.* 531 (2017) 1–9, <https://doi.org/10.1016/j.memsci.2017.02.046>.
- [39] Z. Chen, H. Su, D. Hu, F. Jia, Z. Li, Y. Cui, C. Ran, X. Wang, J. Xu, T. Xiao, X. Li, H. Wang, Effect of organic loading rate on the removal of DMF, MC and IPA by a pilot-scale AnMBR for treating chemical synthesis-based antibiotic solvent wastewater, *Chemosphere* 198 (2018) 49–58.
- [40] C.H. Wei, M. Harb, G. Amy, P.Y. Hong, T. Leiknes, Sustainable organic loading rate and energy recovery potential of mesophilic anaerobic membrane bioreactor for municipal wastewater treatment, *Bioresour Technol* 166 (2014) 326–334, <https://doi.org/10.1016/j.biortech.2014.05.053>.
- [41] Q. Yu, L. Feng, X. Zhen, Effects of organic loading rate and temperature fluctuation on the microbial community and performance of anaerobic digestion of food waste, *Environ Sci Pollut Res Int* 28 (11) (2021) 13176–13187, <https://doi.org/10.1007/s11356-020-11548-8>.
- [42] A. Olubukola, R.K. Gautam, T. Kamilya, S. Muthukumar, D. Navaratna, Development of a dynamic model for effective mitigation of membrane fouling through biogas sparging in submerged anaerobic membrane bioreactors (SAMBRs), *J. Environ. Manage.* 323 (2022), 116151, <https://doi.org/10.1016/j.jenvman.2022.116151>.
- [43] D. Navaratna, V. Jegatheesan, Implications of short and long term critical flux experiments for laboratory-scale MBR operations, *Bioresour Technol* 102 (9) (2011) 5361–5369, <https://doi.org/10.1016/j.biortech.2010.12.080>.
- [44] R.E. Speece, Anaerobic biotechnology for industrial wastewater treatment, *Environmental science & technology* 17(9) (1983) 416A–427A.
- [45] WE Federation, A. Association, Standard methods for the examination of water and wastewater, American Public Health Association (APHA): Washington, DC, USA (2005).
- [46] M. DuBois, K.A. Gilles, J.K. Hamilton, P.A. Rebers, F. Smith, Colorimetric Method for Determination of Sugars and Related Substances, *Anal. Chem.* 28 (3) (2002) 350–356, <https://doi.org/10.1021/ac60111a017>.
- [47] A. Charfi, N. Thongmak, B. Benyahia, M. Aslam, J. Harmand, N.B. Amar, G. Lesage, P. Sridang, J. Kim, M. Heran, A modelling approach to study the fouling of an anaerobic membrane bioreactor for industrial wastewater treatment, *Bioresour Technol* 245 (Pt A) (2017) 207–215, <https://doi.org/10.1016/j.biortech.2017.08.003>.
- [48] E. Metcalf Inc., Wastewater engineering treatment and reuse, McGraw-Hill, New York, 2003, p. 1819.
- [49] M.H. Al-Malack, Determination of biokinetic coefficients of an immersed membrane bioreactor, *J. Membr. Sci.* 271 (1–2) (2006) 47–58.
- [50] N.-J. Jang, M.-H. Hwang, Y.-H. Yeo, W.-G. Shim, I.-S. Kim, The kinetics on the biological reaction in membrane bioreactor (MBR) with gravitational and transverse filtration, *Environ. Eng. Res.* 9 (5) (2004) 238–247.
- [51] H. Nagaoka, S. Yamanishi, A. Miya, Modeling of biofouling by extracellular polymers in a membrane separation activated sludge system, *Water Sci. Technol.* 38 (4–5) (1998) 497–504.
- [52] J. Busch, A. Cruse, W. Marquardt, Modeling submerged hollow-fiber membrane filtration for wastewater treatment, *J. Membr. Sci.* 288 (1–2) (2007) 94–111, <https://doi.org/10.1016/j.memsci.2006.11.008>.
- [53] C.-H. Xing, Y. Qian, X.-H. Wen, W.-Z. Wu, D. Sun, Physical and biological characteristics of a tangential-flow MBR for municipal wastewater treatment, *J. Membr. Sci.* 191 (1–2) (2001) 31–42, [https://doi.org/10.1016/S0376-7388\(01\)00472-0](https://doi.org/10.1016/S0376-7388(01)00472-0).
- [54] M. Lousada-Ferreira, J.B. van Lier, J.H. van der Graaf, Impact of suspended solids concentration on sludge filterability in full-scale membrane bioreactors, *J. Membr. Sci.* 476 (2015) 68–75, <https://doi.org/10.1016/j.memsci.2014.11.012>.
- [55] S.M. Mohan, S. Nagalakshmi, A review on aerobic self-forming dynamic membrane bioreactor: Formation, performance, fouling and cleaning, *J. Water Process Eng.* 37 (2020), 101541, <https://doi.org/10.1016/j.jwpe.2020.101541>.
- [56] M. Pandian, N. Huu-Hao, S. Pazhaniappan, Substrate removal kinetics of an anaerobic hybrid reactor treating pharmaceutical wastewater, *J. Water Sustainability* 1 (3) (2011) 301–312.
- [57] X. Xiao, W. Shi, Z. Huang, W. Ruan, H. Miao, H. Ren, M. Zhao, Process stability and microbial response of anaerobic membrane bioreactor treating high-strength kitchen waste slurry under different organic loading rates, *Int. Biodeter. Biodegr.* 121 (2017) 35–43, <https://doi.org/10.1016/j.ibiod.2017.03.012>.
- [58] T. Inaba, T. Aoyagi, T. Hori, A. Charfi, C. Suh, J.H. Lee, Y. Sato, A. Ogata, H. Aizawa, H. Habe, Long-term acclimatization of sludge microbiome for treatment of high-strength organic solid waste in anaerobic membrane bioreactor, *Biochem. Eng. J.* 154 (2020), 107461, <https://doi.org/10.1016/j.bej.2019.107461>.
- [59] Z. Huang, S.L. Ong, H.Y. Ng, Submerged anaerobic membrane bioreactor for low-strength wastewater treatment: effect of HRT and SRT on treatment performance and membrane fouling, *Water Res* 45 (2) (2011) 705–713, <https://doi.org/10.1016/j.watres.2010.08.035>.
- [60] I. Burman, A. Sinha, Performance evaluation and substrate removal kinetics in an up-flow anaerobic hybrid membrane bioreactor treating simulated high-strength

- wastewater, *Environ Technol* 41 (3) (2020) 309–321, <https://doi.org/10.1080/09593330.2018.1498132>.
- [61] A.D. Grossman, Y. Yang, U. Yogev, D.C. Camarena, G. Oron, R. Bernstein, Effect of ultrafiltration membrane material on fouling dynamics in a submerged anaerobic membrane bioreactor treating domestic wastewater, *Environ. Sci. Water Res. Technol.* 5 (6) (2019) 1145–1156, <https://doi.org/10.1039/c9ew00205g>.
- [62] S. Khan, *Hydrophobicity of Rare-earth Oxide Ceramics and their Application in Promoting Sustained Dropwise Condensation and Corrosion and Fouling Mitigation in Hydropower Systems*, Hydropower Foundation, 2015.
- [63] A. Maghsodi, L. Adlnasab, In-situ chemical deposition as a new method for the preparation of Fe<sub>3</sub>O<sub>4</sub> nanoparticles embedded on anodic aluminum oxide membrane (Fe<sub>3</sub>O<sub>4</sub>@AAO): Characterization and application for arsenic removal using response surface methodology, *J. Environ. Chem. Eng.* 7 (5) (2019), 103288, <https://doi.org/10.1016/j.jece.2019.103288>.
- [64] W. Yang, Q. Guo, D. Duan, T. Wang, J. Liu, X. Du, Y. Liu, S. Xia, Characteristics of flat-sheet ceramic ultrafiltration membranes for lake water treatment: A pilot study, *Sep. Purif. Technol.* 289 (2022), 120677, <https://doi.org/10.1016/j.seppur.2022.120677>.
- [65] E.S. Rigobello, S.X. Campos, E.R.d. Azevedo, A.D.B. Dantas, E.M. Vieira, Comparative characterization of humic substances extracted from freshwater and peat of different apparent molecular sizes, *Revista Ambiente & Água* 12 (2017) 774–785.
- [66] M. Kumar, S.S. Adham, W.R. Pearce, Investigation of seawater reverse osmosis fouling and its relationship to pretreatment type, *Environ. Sci. Tech.* 40 (6) (2006) 2037–2044.
- [67] J.-P. Croué, M. Benedetti, D. Violleau, J. Leenheer, Characterization and copper binding of humic and nonhumic organic matter isolated from the South Platte River: evidence for the presence of nitrogenous binding site, *Environ. Sci. Tech.* 37 (2) (2003) 328–336.
- [68] M. Lee, J. Kim, Membrane autopsy to investigate CaCO<sub>3</sub> scale formation in pilot-scale, submerged membrane bioreactor treating calcium-rich wastewater, *J. Chem. Technol. Biotechnol.* 84 (9) (2009) 1397–1404.
- [69] S. Banerjee, B. Santra, S. Kar, D. Banerjee, S. Ghosh, S. Majumdar, Performance assessment of the indigenous ceramic UF membrane in bioreactor process for highly polluted tannery wastewater treatment, *Environ. Sci. Pollut. Res.* 29 (32) (2022) 48620–48637, <https://doi.org/10.1007/s11356-022-19258-z>.
- [70] N. Fallah, B. Bonakdarpour, B. Nasernejad, M.R. Alavi Moghadam, Long-term operation of submerged membrane bioreactor (MBR) for the treatment of synthetic wastewater containing styrene as volatile organic compound (VOC): Effect of hydraulic retention time (HRT), *J. Hazard. Mater.* 178 (1) (2010) 718–724, <https://doi.org/10.1016/j.jhazmat.2010.02.001>.
- [71] T. Inaba, T. Su, T. Aoyagi, H. Aizawa, Y. Sato, C. Suh, J.H. Lee, T. Hori, A. Ogata, H. Habe, Microbial community in an anaerobic membrane bioreactor and its performance in treating organic solid waste under controlled and deteriorated conditions, *J. Environ. Manage.* 269 (2020), 110786, <https://doi.org/10.1016/j.scitotenv.2021.145799>.
- [72] A. Anzecc, Australian and New Zealand guidelines for fresh and marine water quality, Australian and New Zealand Environment and Conservation Council and Agriculture and Resource Management Council of Australia and New Zealand, Canberra 1 (2000) 1-314.
- [73] Y.A. Skaik, The bread and butter of statistical analysis “t-test”: Uses and misuses, (2015). 10.12669%2Fpjms.316.8984.
- [74] S. Gupta, V. Kapoor, *Fundamentals of mathematical statistics*, Sultan Chand & Sons, 2020.